ANGEWANDTE CHEMIE

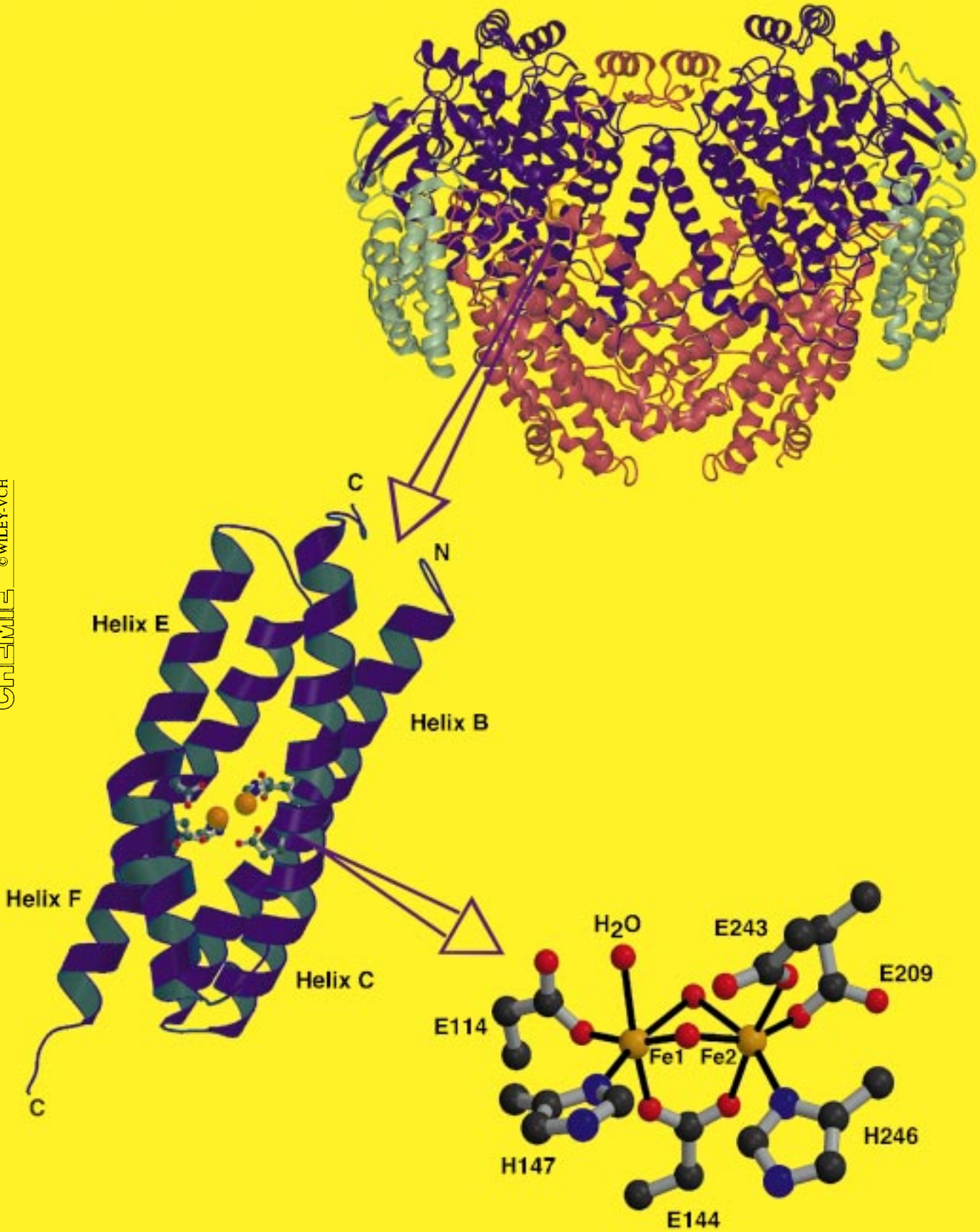

Dioxygen Activation and Methane Hydroxylation by Soluble Methane Monooxygenase: A Tale of Two Irons and Three Proteins**

Maarten Merkx, Daniel A. Kopp, Matthew H. Sazinsky, Jessica L. Blazyk, Jens Müller, and Stephen J. Lippard*

Methanotrophic bacteria are capable of using methane as their sole source of carbon and energy. The first step in methane metabolism, the oxidation of methane to methanol, is catalyzed by a fascinating enzyme system called methane monooxygenase (MMO). The selective oxidation of the very stable C–H bond in methane under ambient conditions is a remarkable feat that has not yet been repeated by synthetic catalysts and has attracted considerable scientific and commercial interest. The best studied MMO is a complex enzyme system that consists of three soluble protein components, all of which are required for efficient catalysis. Dioxygen activation and subsequent methane hydroxylation are catalyzed by a hydroxylase enzyme that contains a non-heme diiron site. A reductase protein accepts electrons from NADH and transfers them to the hydroxylase where they are used for the reductive activation of O_2. The third protein component couples electron and dioxygen consumption with methane oxidation. In this review we examine different aspects of catalysis by the MMO proteins, including the mechanisms of dioxygen activation at the diiron site and substrate hydroxylation by the activated oxygen species. We also discuss the role of complex formation between the different protein components in regulating various aspects of catalysis.

Keywords: bioinorganic chemistry · C–H activation · oxidoreductases · O–O activation · oxygenation

1. Introduction

Methane monooxygenases (MMOs) catalyze the selective oxidation of methane to methanol [Eq. (1)].[1–6]

$$CH_4 + NADH + H^+ + O_2 \longrightarrow CH_3OH + NAD^+ + H_2O \quad (1)$$

This reaction is the essential first step in a metabolic pathway used by methanotrophic bacteria to consume methane as their sole source of carbon and energy (Scheme 1).[7] Methanotrophs reside at the boundary of aerobic and anaerobic environments, where both methane and dioxygen exist. Methane is produced by methanogenic bacteria, which reduce CO_2 to CH_4 in various anaerobic surroundings such as oceans, lakes, and wetlands.[8] Methanotrophs play an essential role in the global carbon cycle by limiting the amount of methane, a more potent greenhouse gas than carbon dioxide, that reaches the atmosphere.[9]

Virtually all methanotrophs express a membrane-bound, particulate form of MMO (pMMO).[10, 11] This 94-kDa enzyme contains about 12–15 copper atoms distributed between two distinct kinds of sites. It has been hypothesized that one of the copper clusters serves as the active site for methane hydroxylation and the other as an electron carrier.[12–16] Detailed characterization of pMMO has been hampered by its instability and by difficulties in purification. Some methanotrophs can also express a second, soluble type of MMO (sMMO) under conditions of low copper availability. sMMO is much more stable and easier to purify, and has therefore attracted considerable attention. The active site of sMMO contains a non-heme diiron center and, in contrast to pMMO, can accommodate a wide variety of hydrocarbon substrates besides methane. Included are saturated and unsaturated, linear, branched, and cyclic hydrocarbons up to about C_8, as well as aromatic, heterocyclic, and chlorinated compounds.[9, 17–22] Because of this broad spectrum of oxidizable substrates, methanotrophic bacteria can assist in bioremediation of the environment, such as in the removal of petroleum products from beaches contaminated by oil tanker spillage.[23] The efficient conversion of methane into methanol, the signature reaction of MMOs, is also of commercial interest.

[*] Prof. Dr. S. J. Lippard, Dr. M. Merkx, D. A. Kopp, M. H. Sazinsky, J. L. Blazyk, Dr. J. Müller
Department of Chemistry
Massachusetts Institute of Technology
77 Massachusetts Avenue 18-590
Cambridge, MA 02139 (USA)
Fax: (+1) 617-258-8150
E-mail: lippard@lippard.mit.edu

[**] A list of abbreviations can be found in Section 7.

  1433-7851/01/4015-2783 $ 17.50+.50/0

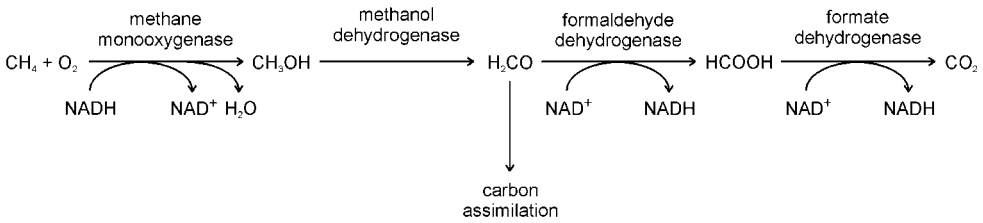

Scheme 1. Metabolic pathway for methane oxidation in *Methylococcus capsulatus* (Bath).

A liquid derivative of natural gas would be more economical to transport, an important consideration for the exploitation of natural gas resources in remote areas. Whereas the successful application of the MMO enzyme on an industrial scale is doubtful, chemical insights gathered from enzymological studies could guide the development of better synthetic catalysts.

Soluble MMO is a complex three-component system (Figure 1).[24–27] sMMO systems isolated from *Methylococcus capsulatus* (Bath) and *Methylosinus trichosporium* OB3b have been investigated extensively and two of their three component proteins have been structurally characterized.[28–33] Oxidation of methane by dioxygen occurs at a carboxylate-bridged diiron center located in the α subunit of the hydroxylase protein MMOH, a 251-kDa $\alpha_2\beta_2\gamma_2$ heterodimer. Electrons

M. Merkx S. J. Lippard J. Müller

D. A. Kopp J. L. Blazyk M. H. Sazinsky

Maarten Merkx (Drs in Chemistry, 1995, University of Nijmegen, The Netherlands; PhD in Chemistry, 1999, University of Amsterdam, The Netherlands) did his graduate research with Professor Bruce A. Averill studying the mechanistic role of the diiron center in purple acid phosphatase. He is presently a Human Frontier of Science Program postdoctoral fellow in Professor Lippard's group, working on the mechanism of methane monooxygenase. His research interest is in the field of metalloenzyme catalysis.

Daniel A. Kopp received a BS degree in Chemistry and Biology from the College of William and Mary, Williamsburg, Virginia, in 1997. While there he researched solvent effects on conformational equilibria in small amides under the supervision of Professor Kathleen M. Morgan. When he is not in the lab, Dan enjoys hiking, playing guitar, and spending time with his wife Karen.

Matthew H. Sazinsky received a BS degree in Chemistry from Haverford College, Haverford, Pennsylvania, in 1999. While there he investigated the functional role of zinc in porphobilinogen synthase under the supervision of Professor Robert C. Scarrow and Dr. Eileen K. Jaffe (Fox Chase Cancer Center, Philadelphia, Pennsylvania). He is currently studying component interactions in sMMO. His research interests are in structural biology and metalloenzymology.

Jessica L. Blazyk received a BS degree in chemistry from the Honors Tutorial College at Ohio University (Athens, Ohio) in 1996. As an undergraduate, she performed research on the mechanism of manganese catalase in the laboratory of Professor James E. Penner-Hahn at the University of Michigan in Ann Arbor, Michigan. She is currently a Howard Hughes Medical Institute predoctoral fellow in Professor Lippard's group, studying electron transfer reactions in the sMMO system.

Jens Müller studied chemistry at the University of Dortmund and at University College, London. He received his PhD in 1999 under the supervision of Professor Bernhard Lippert for studies of platinum-stabilized, parallel-stranded DNA and stabilization of rare tautomers of nucleobases. Currently, he is working in the groups of Professor Lippard (MIT) and Professor Gerhard Wagner (Harvard Medical School) as a Feodor-Lynen postdoctoral fellow. His present research interests include the determination of solution structures of proteins.

Stephen J. Lippard is the Arthur Amos Noyes Professor of Chemistry at the Massachusetts Institute of Technology and is Head of the Chemistry Department. A member of the National Academy of Sciences, the National Institute of Medicine, and the American Academy of Arts and Sciences, his research activities span the fields of inorganic and biological chemistry. Working to unravel the mysteries of soluble methane monooxygenase has been one of his scientific passions for more than a decade.

Overall reaction: $CH_4 + O_2 + 2H^+ + 2e^- \longrightarrow CH_3OH + H_2O$

Figure 1. Schematic view of the three protein components that form the soluble methane monooxygenase enzyme and their roles in catalysis. Only one of two non-heme diiron centers in the MMOH dimer is depicted.

for this reaction are provided by a reductase protein, MMOR, which oxidizes NADH and transfers its electrons to MMOH. Efficient catalysis requires the presence of a third protein, MMOB, which serves several regulatory roles.

An important reason for the scientific interest in sMMO is its unique ability to oxidize the very stable C–H bond in methane. This feat distinguishes sMMO from other monooxygenase enzymes such as cytochrome P450.[34] Cytochrome P450 and sMMO represent two different solutions to the problem of dioxygen activation for hydrocarbon oxidation.[35] Cytochrome P450 enzymes activate dioxygen at a cysteine-ligated Fe–porphyrin unit, whereas non-heme diiron centers are employed by sMMO and related multicomponent monooxygenases. Similar carboxylate-bridged dinuclear iron centers occur in other proteins, where they perform a wide variety of functions. Included are the reversible binding of O_2 in hemerythrin, formation of a stable radical in class I ribonucleotide reductase, desaturation of fatty acid chains by stearoyl-ACP Δ^9 desaturase, oxidation and storage of iron in ferritin, and possibly dioxygen sensing in the bacterial chemotaxis protein DcrH.[3, 36–40] The diversity of chemical reactivity displayed by non-heme diiron centers rivals that of heme groups, and both often serve similar functions in metalloproteins.[35] Understanding the factors that tune these iron centers to perform a specific function is of fundamental importance.[41]

Another aspect of sMMO catalysis that has attracted much attention is the mechanism by which catalysis is regulated. The activation of unreactive C–H bonds requires the generation of a potent activated oxygen intermediate, which necessitates the tight regulation of electron, proton, and substrate delivery. An important method of regulation employed by multicomponent enzyme systems such as sMMO is to separate physically the site of electron entry from the site where molecular oxygen is reductively activated. In addition, several more subtle types of regulation have been identified.

Soluble MMO thus represents a wonderful system for studying the fundamental chemistry of dioxygen activation and of methane hydroxylation at the diiron site, as well as the regulatory mechanisms employed by a multicomponent oxygenase, including long-range electron transfer. Both aspects of MMO catalysis are discussed in this review. In Section 2, we take a closer look at the three components of sMMO with emphasis on their structures. Section 3 presents key information obtained by time-resolved spectroscopic techniques on the nature of several catalytic intermediates, both for the reductive activation of dioxygen and for electron transfer from NADH through MMOR to MMOH. The mechanism of substrate hydroxylation has been evaluated both with the use of molecular reporter probes and by calculations at the density functional theory (DFT) level (Section 4). Section 5 describes the role of component interactions in the regulation of various aspects of catalysis. As we shall see, biological methane oxidation is very much a tale of two irons and three proteins.

2. Protein Components of Soluble Methane Monooxygenase

The three protein components that form the soluble MMO enzyme system, MMOH, MMOR, and MMOB, have been characterized by a variety of kinetic, spectroscopic, and structural techniques. Before we describe structures of these components in more detail, some general features of sMMO and related multicomponent oxygenases warrant discussion.

The hydroxylase enzyme MMOH is a 251-kDa dimer of three subunits in an $\alpha_2\beta_2\gamma_2$ configuration (α, 60.6 kDa; β, 45.0 kDa; γ, 19.8 kDa).[24, 26] Each α subunit contains a carboxylate- and hydroxo-bridged dinuclear iron center, where dioxygen activation and methane hydroxylation occur. MMOR is a 38.5-kDa iron–sulfur flavoprotein that shuttles electrons from NADH through its flavin adenine dinucleotide (FAD) and [2Fe–2S] cofactors to the hydroxylase active site.[27, 42, 43] MMOB (15.9 kDa) contains no prosthetic groups and modulates MMO reactivity by forming specific complexes with the hydroxylase that indirectly affect the structure and reactivity of the diiron site.[24, 27, 44–50] In *M. trichosporium* OB3b, MMOH, MMOB, and MMOR represent 12, 0.5, and 0.1–0.3 wt%, respectively, of soluble protein in a cell-free extract prepared under low copper concentrations. Therefore, on a molar basis, approximately equivalent concentrations of MMOH and MMOB are present in the cell, whereas the reductase concentration is only 10% that of the other components.[24] Similar results have been reported for soluble cell extracts from *Methylocystis* sp. strain WI14.[51]

The genes encoding the sMMO proteins of *M. capsulatus* (Bath),[52–54] *M. trichosporium* OB3b,[30, 55, 56] *Methylocystis* sp. strain M,[57] *Methylocystis* sp. strain WI14,[51] and *Methylomonas* sp. strains KSPIII and KSWIII have been identified and sequenced.[58] These genes are clustered on a 5.5-kb operon, comprising *mmoX*, *mmoY*, *mmoB*, *mmoZ*, *orfY*, and *mmoC*, which code, respectively, for $MMOH_\alpha$, $MMOH_\beta$, MMOB, $MMOH_\gamma$, a protein of unidentified function (OrfY, 12 kDa), and MMOR (Figure 2). Expression in *M. capsulatus* (Bath) is controlled by a single σ^{70}-dependent, copper-regulated pro-

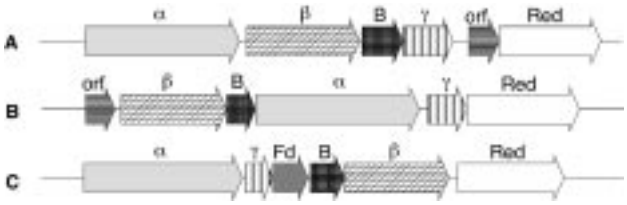

Figure 2. Organization of the sMMO operon (**A**) and operons of related multicomponent monooxygenases (**B**,**C**). Arrangement **B** occurs for phenol hydroxylase and benzene/toluene-2-monooxygenase, whereas arrangement **C** is found for toluene-3-monooxygenase, toluene-4-monooxygenase, and *Xanthobacter* alkene monooxygenase. The components are encoded as follows: α, β, and γ: hydroxylase (or epoxidase) subunits; B: coupling protein; Red: reductase; Fd: ferredoxin; orf: open reading frame (DmpK protein in phenol hydroxylase). Reprinted with permission from ref. [54]. Copyright (2000) Blackwell Science.

moter located upstream of the *mmoX* gene, such that in the native bacterium the sMMO system is produced only under conditions of low copper concentration.[59] Transcription of the *M. trichosporium* OB3b sMMO genes is directed from a σ^{54}-like promoter upstream of *mmoX* and a σ^{70}-like promoter located in the intercistronic region between *mmoX* and *mmoY*.[59, 60]

Amino acid sequences of these six sets of sMMO proteins are universally conserved as follows: $MMOH_{\alpha}$, 73.6%; $MMOH_{\beta}$, 46.8%; MMOB, 55.6%; $MMOH_{\gamma}$, 35.7%; OrfY, 19.4%; and MMOR, 37.4%. The function of OrfY has remained unclear; the protein has not been isolated from any of the native organisms and exhibits no significant homology with other known proteins.[54, 61] Although the overall percent identity for the putative OrfY products is fairly low (19.4%), there is a central region with a significantly greater number of conserved residues (44.4%). Very recently we have expressed OrfY from *M. capsulatus* (Bath) in *E. coli*. In contrast to an earlier report,[11] Western blot analysis of *M. capsulatus* (Bath) soluble cell extracts with an antibody to OrfY clearly showed the presence of the OrfY protein, albeit at much lower levels than that of MMOH (1–2%). Recombinant OrfY inhibits the MMO-catalyzed epoxidation of propene, probably by binding directly to MMOH.[62] These results clearly suggest that OrfY plays a functional role in the sMMO system. One possibility is that the protein participates in the assembly of the hydroxylase diiron centers, a function assigned to a protein of similar size but no apparent sequence homology, DmpK, in the related phenol hydroxylase from *Pseudomonas* sp. CF600.[63] Despite our new evidence for a fourth component, the title of this review is still appropriate, for we have no reason at present to suspect that OrfY functions in sMMO catalysis.

Several monooxygenases, including benzene/toluene-2-monooxygenase,[64] toluene-3-monooxygenase,[65, 66] toluene-4-monooxygenase,[67–70] phenol hydroxylase,[71–74] and alkene monooxygenase,[75–80] are quite similar to sMMO. All of these protein systems contain a hydroxylase with two or three subunits housing a non-heme carboxylate-bridged diiron center, a reductase, and a coupling protein. In addition, dioxygen is the oxidant in each of the hydroxylation or epoxidation reactions they catalyze. Sequence alignments demonstrate that many amino acid residues are highly conserved across this set of proteins, especially at the diiron active site of the hydroxylase α subunit.[54, 66, 68, 80–82] sMMO is thus far the best studied member of these oxygenases.

High-yield recombinant expression systems have been developed for both MMOB and, more recently, MMOR in *E. coli*.[31, 54, 61, 83, 84] The ability to express MMOR in high yield is particularly important for structural studies because only small amounts of this protein can be isolated from the native organism. Recombinant expression of MMOH has proved to be more challenging. MMOH expressed in *E. coli* does not fold properly, which results in the formation of inclusion bodies.[11, 85] Plasmids carrying the *M. trichosporium* OB3b MMOH genes yield active enzyme when expressed in certain strains of *Pseudomonas* or in native *M. trichosporium* OB3b cells in which the chromosomal copy of the *mmoX* gene has been disrupted.[86–89] Purification and characterization of recombinant MMOH and mutant MMOH proteins from these expression systems have not been reported, however.

2.1. MMOH

Although all three components of sMMO are necessary for efficient catalysis, MMOH alone can activate dioxygen and hydroxylate various hydrocarbons in the absence of the other components when it is chemically reduced to the diferrous state.[24, 50] Therefore, the chemistry of dioxygen activation and substrate hydroxylation takes place at the diiron centers in the α subunits of MMOH. Much effort has been devoted to the characterization of the structural features of the diiron site in its various oxidation states and in the transient intermediates of the dioxygen activation reaction. In this section we first present the most important structural insights gained from spectroscopic studies. This discussion is followed by an examination of X-ray crystal structure determinations of MMOH in a variety of crystal forms, oxidation states, and substrate analogue and product complexes, which together provide insight into the dynamics of the MMOH active site.

2.1.1. Spectroscopic Characterization of MMOH

The diiron center of MMOH has been thoroughly characterized by a variety of spectroscopic techniques including EXAFS,[90–95] EPR,[44, 46, 47, 92, 96–100] ENDOR/ESEEM,[47, 99, 101–107] optical,[24, 92] MCD,[108–110] and Mössbauer techniques.[24, 47, 50, 92, 111] The spectroscopic properties of non-heme iron sites in enzymes, including those of MMOH, have recently been reviewed.[39] Here we focus on studies most relevant to enzyme catalysis (see Table 1).

The diiron site of MMOH can exist in three stable oxidation states, $Fe^{III}Fe^{III}$ ($MMOH_{ox}$), $Fe^{III}Fe^{II}$ ($MMOH_{mv}$), and $Fe^{II}Fe^{II}$ ($MMOH_{red}$). In $MMOH_{ox}$, the high-spin ferric irons are antiferromagnetically coupled to form a diamagnetic ground state that is EPR silent.[92, 96, 111, 112] Unlike hemerythrin, ribonucleotide reductase, and stearoyl-ACP Δ^9 desaturase, proteins that have a bridging oxo group in the diferric oxidation state,[39, 81, 113–116] antiferromagnetic spin exchange in $MMOH_{ox}$ is mediated by more weakly coupling bridging ligands. EXAFS studies of $MMOH_{ox}$ showed no evidence for

Table 1. Spectroscopic properties of MMO hydroxylase (H) in the presence and absence of MMOB (B).

	Source[a]	EPR/ENDOR		Mössbauer					EXAFS	
		EPR g values	Hyperfine coupling	J [cm^{-1}][l]	δ(Fe 1) [$mm\,s^{-1}$]	ΔE_Q(Fe 1) [$mm\,s^{-1}$]	δ(Fe 2) [$mm\,s^{-1}$]	ΔE_Q(Fe 2) [$mm\,s^{-1}$]	Fe–Fe distance	Other distances
H_{ox}	MCB	1.94, 1.87, 1.72 1.82, 1.77, 1.68[b,c]			0.51 0.72[n,o]	1.12 1.46[n,o]	0.50 0.47[n,o]	0.79 1.33[n,o]	3.42 Å[h]	1st O/N shell at 2.06 – 2.09 Å
H_{ox}	MTO	1.94, 1.86, 1.79 1.85, 1.75, 1.7[b,d]		-7 ± 3[f]	0.51[f]	1.16[f]	0.50[f]	0.87[f]	60 % 3.01 Å 40 % 3.36 Å[q]	2 O/N at 1.96 Å 3 O/N at 2.09 Å
$H_{ox}+B$	MCB	1.94, 1.86, 1.79 1.82, 1.77, 1.68[b,c]							3.39 Å[r]	same as $MMOH_{ox}$
$H_{ox}+B$	MTO	1.97, 1.86, 1.75 1.90, 1.79, 1.59[b,d]							same as $MMOH_{ox}$[q]	
H_{mv}	MCB	1.94, 1.87, 1.72[c]	14 – 30 MHz (μ-OH) 8 MHz ($FeOH_{(2)}$)[j]	-32[h]					3.42 Å[h,r,s]	
H_{mv}	MTO	1.94, 1.86, 1.75[d,e,f]	13 – 23 MHz (μ-OH) 8 MHz ($FeOH_{(2)}$)[k]	-30[g]	0.48[p,f]	-1.3[p,f]	1.19[p,f]	2.4[p,f]		
$H_{mv}+B$	MCB	1.88, 1.77, 1.63[c]								
$H_{mv}+B$	MTO	1.86, 1.77, 1.62[f,g]		-5[g]						
H_{red}	MCB	15[h]			1.3[n,o]	2.8[n,o]	1.3[n,o]	2.8[n,o]	no Fe–Fe scattering[r,s]	
H_{red}	MTO	16[e,f,g]		0.35[m]	1.3[f,n]	3.0[f,n]	1.3[f,n]	2.7[f,n]		
$H_{red}+B$	MTO	16 (sharper than H_{red})[g,h]								

[a] MCB: *Methylococcus capsulatus* (Bath); MTO: *Methylosinus trichosporium* OB3b. [b] EPR parameters for cryogenically reduced $MMOH_{ox}$ species. [c] Ref. [100]. [d] Ref. [98]. [e] Ref. [111]. [f] Ref. [47]. [g] Ref. [44]. [h] Ref. [92]. [i] Ref. [46]. [j] Ref. [102]. [k] Ref. [103]. [l] Values are reported using the convention $H=-2JS_1S_2$. [m] Ref. [97]. [n] Measured at 4 K. [o] Ref. [50]. [p] Measured at 150 K. [q] Ref. [94]. [r] Ref. [93]. [s] Ref. [91].

short 1.75 – 1.80 Å Fe–O bonds characteristic of $\{Fe_2(\mu\text{-oxo})\}^{4+}$ units, and optical spectra similarly lacked absorbances at 350 and 500 – 600 nm that are typical of oxo-bridged diferric complexes.[24, 39, 91, 94] Analysis of one-electron reduced analogues of $MMOH_{ox}$, obtained after cryoreduction of frozen $MMOH_{ox}$ samples by γ-irradiation, has allowed characterization of small molecule-bound and protein component-bound forms of $MMOH_{ox}$ by EPR spectroscopy.[98, 100, 117, 118] These studies demonstrate that the diiron site of $MMOH_{ox}$ is affected by binding of MMOB but not of MMOR. Product alcohols such as methanol and phenol bind to the dimetallic center, whereas glycerol and DMSO, an inhibitor, bind only in the presence of MMOB. Binding of phenol to $MMOH_{ox}$ has also been observed by resonance Raman spectroscopy.[119]

Structural studies of the mixed-valent oxidation state are of limited direct relevance to the catalytic mechanism, because $MMOH_{mv}$ does not react with dioxygen. Moreover, two-electron transfer to $MMOH_{ox}$ is favored in the ternary MMOH – MMOB – MMOR complex.[2, 45, 96, 120] Antiferromagnetic coupling between high-spin Fe^{III} and high-spin Fe^{II} results in an $S=1/2$ ground state, which gives rise to a rhombic EPR spectrum with $g<2$.[47, 96, 112] Advanced pulsed EPR techniques have been used to study the binding of substrate/product-like small molecules to the diiron center in $MMOH_{mv}$ and to monitor the effects of component interactions on its structure. Signals corresponding to a bridging hydroxo group and water or hydroxide ion bound at a terminal position have been identified with ENDOR/ESEEM spectroscopy.[101–103] Hyperfine couplings between the diiron center and ^2H- and ^{13}C-labeled DMSO, ^{13}C-labeled MeOH, and acetate reveal that all three molecules bind directly to the diiron center.[99, 101, 106]

Mössbauer spectroscopy demonstrates that both iron atoms are high-spin ferrous and weakly ferromagnetically coupled in the reduced diiron(II) oxidation state.[47, 92, 111] The resulting integer spin system has a low-lying doublet that is split in zero applied field by an energy with an average value in the microwave range, giving rise to a very characteristic EPR absorption around $g=16$.[97, 105, 108] The $g=16$ signal of $MMOH_{red}$ has proved to be very useful for monitoring the reaction of $MMOH_{red}$ with O_2 (see Section 3). MCD spectra are consistent with the presence of two five-coordinate, square-pyramidal ferrous centers.[108–110] MMOB binding affects primarily the coordination geometry of one of the two Fe atoms. In contrast to $MMOH_{ox}$, substrate/product-like molecules such as MeOH, DMSO, and MeCN do not seem to bind to $MMOH_{red}$. Products such as MeOH and phenol that bind to $MMOH_{ox}$ are thus released when $MMOH_{ox}$ is reduced to $MMOH_{red}$, which facilitates substrate binding in the next catalytic cycle.

2.1.2. Crystal Structures of MMOH

The crystal structure of $MMOH_{ox}$ from *M. capsulatus* (Bath), reported in 1993, provided the first high-resolution view of the MMOH protein structure and the details of its diiron site.[28, 121] The elucidation of the MMOH structure laid the foundation for much of our current knowledge about transient intermediates in the activation of dioxygen, allowed for the calibration of theoretical calculations on MMOH, and suggested modes for substrate access and component interactions. Since then, crystal structures of MMOH have been reported for $MMOH_{ox}$ from *M. trichosporium* OB3b,[30] and for MMOH from *M. capsulatus* (Bath) in different crystal forms, oxidation states, and in the presence of various

substrates and products.[28, 29, 33, 121–123] Table 2 lists 19 MMOH samples for which structures have been crystallographically determined. Since the two αβγ protomers from the *M. capsulatus* (Bath) crystals are not related by crystallographic symmetry, the 17 *M. capsulatus* (Bath) structures represent a collection of 34 independent active site geometries. Such a collection of structures of the same protein provides important information about the flexibility of amino acid side chains at the active site. These structures reveal conformational changes that may occur during catalysis and its regulation. Rather than describing all of these structures in detail, we focus here on their common features and discuss differences that may be relevant to MMOH function. In general, the global conformation of the protein remains unperturbed among the various forms of MMOH, with changes concentrated at the diiron center and a few residues at or near the active site. We restrict our discussion to structures obtained for MMOH from *M. capsulatus* (Bath), but the *M. trichosporium* OB3b active site geometry and overall protein structure are quite similar.

The architecture of MMOH is that of a heart-shaped $\alpha_2\beta_2\gamma_2$ dimer (Figure 3) and consists almost entirely of α-helical secondary structure. The subunits are arranged as two αβγ protomers that are related by a noncrystallographic, twofold symmetry axis. Extensive helical contacts between the α and β subunits of each protomer are responsible for dimer formation. At the interface between each of the monomers, a canyon region with dimensions of approximately 80 Å × 40 Å × 20 Å is formed. The γ subunits flank the two sides of the hydroxylase and are not involved in dimer formation.

The diiron centers reside in four-helix bundles that are formed by helices B, C, E, and F in the core of the α subunit (Figure 3). Helices B and E each contribute a glutamate residue (Glu114, Glu209) to the diiron center, whereas helices C and F each donate two iron-coordinating residues in the form of a Glu-Xxx-Xxx-His motif. The remainder of the coordination sphere is occupied by solvent-derived ligands.

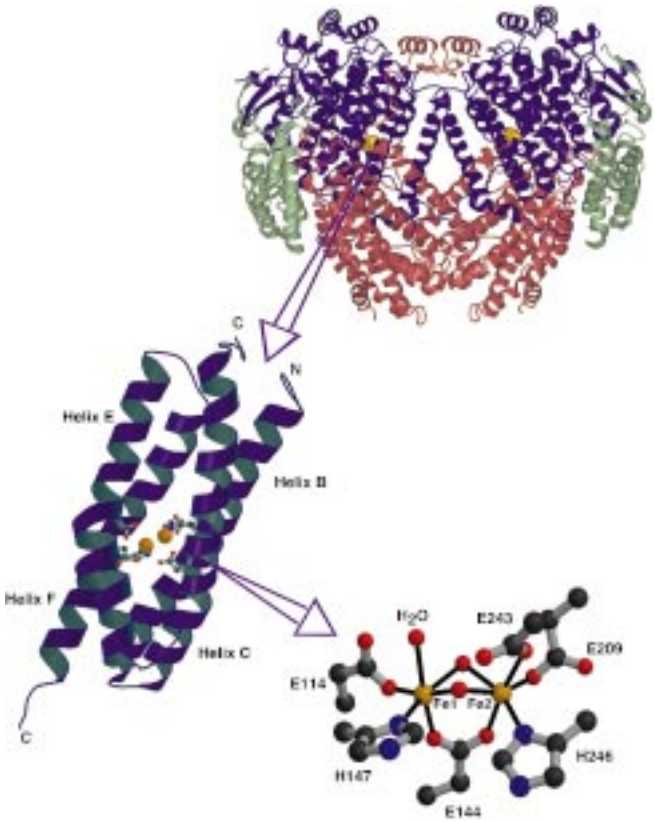

Figure 3. Three structural levels in MMOH from *M. capsulatus* (Bath). Top: Overall fold of MMOH with the twofold symmetry axis running vertically. α: purple; β: red; γ: green. Middle: ribbon diagram of four-helix bundle with Glu (E) and His (H) ligands depicted in ball-and-stick form. Bottom: ball-and-stick model of the diiron center in $MMOH_{ox}$. This figure was produced with the programs Molmol,[231] Molscript,[232] and Raster3d.[233]

Very similar structures occur in other enzymes that use a carboxylate-bridged diiron center to activate dioxygen, including the R2 subunit of class I ribonucleotide reductase and stearoyl-ACP Δ^9 desaturase.[113, 124, 125]

Table 2. Crystal structures of MMOH.

Species[a]	Redox state[b]	Experimental conditions	Crystal form	Resolution [Å]	PDB reference
MCB	ox	277 K	Form I	2.20	1MMO[28]
MCB	ox	113 K	Form I	1.70	pending[29]
MCB	ox	100 K	Form II	1.96	1FZ1[33]
MCB	red	100 K	Form I	1.70	1MTY[122]
MCB	red	reduced in crystal, 100 K	Form II	2.15	1FYZ[33]
MCB	red	grown from $MMOH_{red}$, 100 K	Form II	2.40	1FZ5[33]
MCB	mv	reduced in crystal, 100 K	Form II	2.15	1FZ2[33]
MCB	mv	grown from $MMOH_{mv}$, 100 K	Form II	2.07	1FZ0[33]
MCB	ox	methanol soaked, 100 K	Form II	2.05	1FZ6[123]
MCB	ox	ethanol soaked, 100 K	Form II	1.96	1FZ7[123]
MCB	ox	DMSO soaked, 100 K	Form I	1.70	pending[224]
MCB	ox	100 K, xenon pressurized	Form I	3.30	1FZI[129]
MCB	ox	100 K, xenon pressurized	Form II	2.60	1FZH[129]
MCB	ox	dibromomethane grown, 100 K	Form II	2.10	1FZ8[129]
MCB	ox	iodoethane grown, 100 K	Form II	2.30	1FZ9[129]
MCB	ox	pH 8.5 soaked, 100 K	Form II	2.38	1FZ4[33]
MCB	ox	pH 6.2 soaked, 100 K	Form II	2.03	1FZ3[33]
MTO	ox	291 K	Form I	2.00	1MHY[30]
MTO	ox	291 K	Form II	2.70	1MHZ[30]

[a] MCB: *Methylococcus capsulatus* (Bath); MTO: *Methylosinus trichosporium* OB3b. [b] Oxidation states: ox, $Fe^{III}Fe^{III}$; red, $Fe^{II}Fe^{II}$; mv, $Fe^{III}Fe^{II}$.

Figure 4 illustrates the diiron center geometries as they appear in crystallographically characterized forms of MMOH. In all $MMOH_{ox}$ structures (Figure 4A–D), both iron atoms have distorted octahedral environments. Fe1 is invariably coordinated by His147, monodentate Glu114, and a terminal water molecule, while Fe2 is coordinated by His246 and monodentate Glu209 and Glu243. Flexibility occurs in the positioning of Glu243, which can form hydrogen bonds to the bridging hydroxide ion or to the terminal water coordinated to Fe1. The iron atoms are bridged by Glu144 (unsymmetrically), a hydroxide ion, and a third ligand. The identity of the third bridging ligand, and with it the Fe–Fe distance, is variable. Bridging water,[29] hydroxide,[30] $H_3O_2^-$,[33] acetate,[28] and formate[33] groups have all been reported in this third position, depending on crystal form, protomer, species, and temperature of data collection. Different ligands can even occupy this bridging position for two protomers in the same molecule of MMOH, indicating that subtle conformational differences between the two protomers can affect the binding affinity of this site. Such flexibility is consistent with this site being the locus of dioxygen activation and methane hydroxylation,[29] a hypothesis supported recently by the finding that both MeOH and EtOH bind at this position (Figure 4I–J).[123]

Significant changes occur at the diiron center upon reduction to the diferrous state.[28, 29, 33] The most notable change is in Glu243, which undergoes a carboxylate shift that displaces the bridging hydroxide ion and forms a bidentate chelating interaction with Fe2 and a single bond to Fe1 (Figure 4E, F). A similar carboxylate bridging mode has recently been observed for the corresponding diferrous centers of D84E and azide-soaked F208A/Y122F mutants of the R2 protein of ribonucleotide reductase.[126, 127] Some variability is observed for the water/hydroxide ligand that occupies the bridging site distal to the two histidine residues, the coordination of which can change from symmetric to weak, asymmetric binding. The distance between the Glu144 oxygen atom and Fe2 decreases from 2.6 Å to 2.3 Å, thereby shifting the carboxylate coordination mode of this ligand from semi-bridging in $MMOH_{ox}$ to bridging in $MMOH_{red}$.

Based on these structures, dioxygen binding most likely occurs by substitution of the weakly coordinating bridging water molecule distal to the histidines. This site directly faces a hydrophobic cavity adjacent to the diiron center. It should be remembered, however, that $MMOH_{red}$ is not very reactive in the absence of MMOB,[49] and that the geometry of the $MMOH_{red}$ active site that reacts with O_2 may differ from that seen in any of the crystal structures.

The diiron centers in $MMOH_{mv}$ and $MMOH_{DMSO}$, formed by soaking $MMOH_{ox}$ crystals with the inhibitor DMSO (10 Vol.%), are similar and severely distorted compared to those of $MMOH_{ox}$ and $MMOH_{red}$ (Figure 4G, H).[29, 33] Although neither structure is directly relevant to MMO catalysis, they provide additional insight into the geometric variability that is possible for the carboxylate-bridged diiron centers in MMOH. In both structures the coordination at Fe1 remains unperturbed, whereas that of Fe2 differs markedly, with Fe2 moving 1 Å perpendicular to the Fe–Fe vector. In the $MMOH_{mv}$ structure, Fe2 is four coordinate, with Glu209, Glu243, His246, and μ-OH serving as monodentate ligands. Bidentate coordination of Glu243 and the coordination of a terminal water molecule afford octahedral geometry at Fe2 in $MMOH_{DMSO}$.

A recurring observation is that the coordination environment at Fe2 is much more flexible than that at Fe1. Comparison of individual B factors reveals considerably more thermal motion at Fe2, and recent work indicates that, under certain conditions, Fe2 is bound less tightly than Fe1.[33] We therefore conclude that Fe2 is most likely the iron atom that is more affected by MMOB binding. As argued previously from CD/MCD data,[108–110] only one of the two iron atoms is significantly affected when the coupling protein interacts with the hydroxylase. MMOB may affect the conformation of Fe2 by altering the conformation of the surface-exposed helices E and F, which contain all of the amino acids (Glu243, His246, and Glu209) that coordinate to Fe2.

The MMOH protein serves not only to supply ligands for the two iron atoms. In order for chemistry to occur at the diiron center, electrons, dioxygen, and hydrocarbon substrates all need to be provided through processes that are tightly regulated. A sequence alignment analysis of sMMOs, toluene monooxygenases, alkene monooxygenases, and phenol hydroxylases reveals a universally conserved hydrogen-bonding network extending outward from the diiron site to the hydroxylase surface.[54] This network includes the iron-coordinating histidine residues as well as Tyr67 and Lys74 at the protein exterior on helix A in the MMOH canyon and located $\sim$10 Å from the diiron site (Figure 5). A similar hydrogen bonding network is present in the R2 protein of ribonucleotide reductase, where it is proposed to be involved in electron transfer.[128] It is possible that electron injection into MMOH from MMOR occurs along this pathway.

The MMO active site contains a hydrophobic substrate-binding pocket at a site distal to the histidines with a volume of approximately 185 $Å^3$. This pocket favors the binding of hydrophobic guests, such as methane and dioxygen. Several possibilities have been considered for substrate entry into and product egress from the active site cavity.[122, 129] The shortest and most direct route for substrate entry into the cavity is through a gap between helices E and F. Conformational changes in these helices, altered side-chain rotamer conformations due to normal protein breathing, or MMOB binding may potentially allow substrate to "wiggle" its way into the active site. A comparison of the structures of $MMOH_{ox}$ and $MMOH_{red}$ does reveal slight conformational differences for these helices.[33]

A different mode of entry for substrates into the active site would involve a series of movements through some of the five hydrophobic cavities identified in the α subunit (Figure 6). A potential route would traverse cavities 3 and 2 running from the surface of the protein through the hydrophobic core of the α subunit to active site cavity 1.[33, 122] Crystallographic studies with xenon-pressurized form I and form II $MMOH_{ox}$ crystals revealed localization of ordered Xe in cavity 2.[129] Because the van der Waals radius of Xe is almost identical to that of methane ($\sim$2.15 Å), its binding in cavity 2 indicates that the buried hydrophobic pockets of the α subunit should be accessible to the natural substrate. Leu110, which acts as a

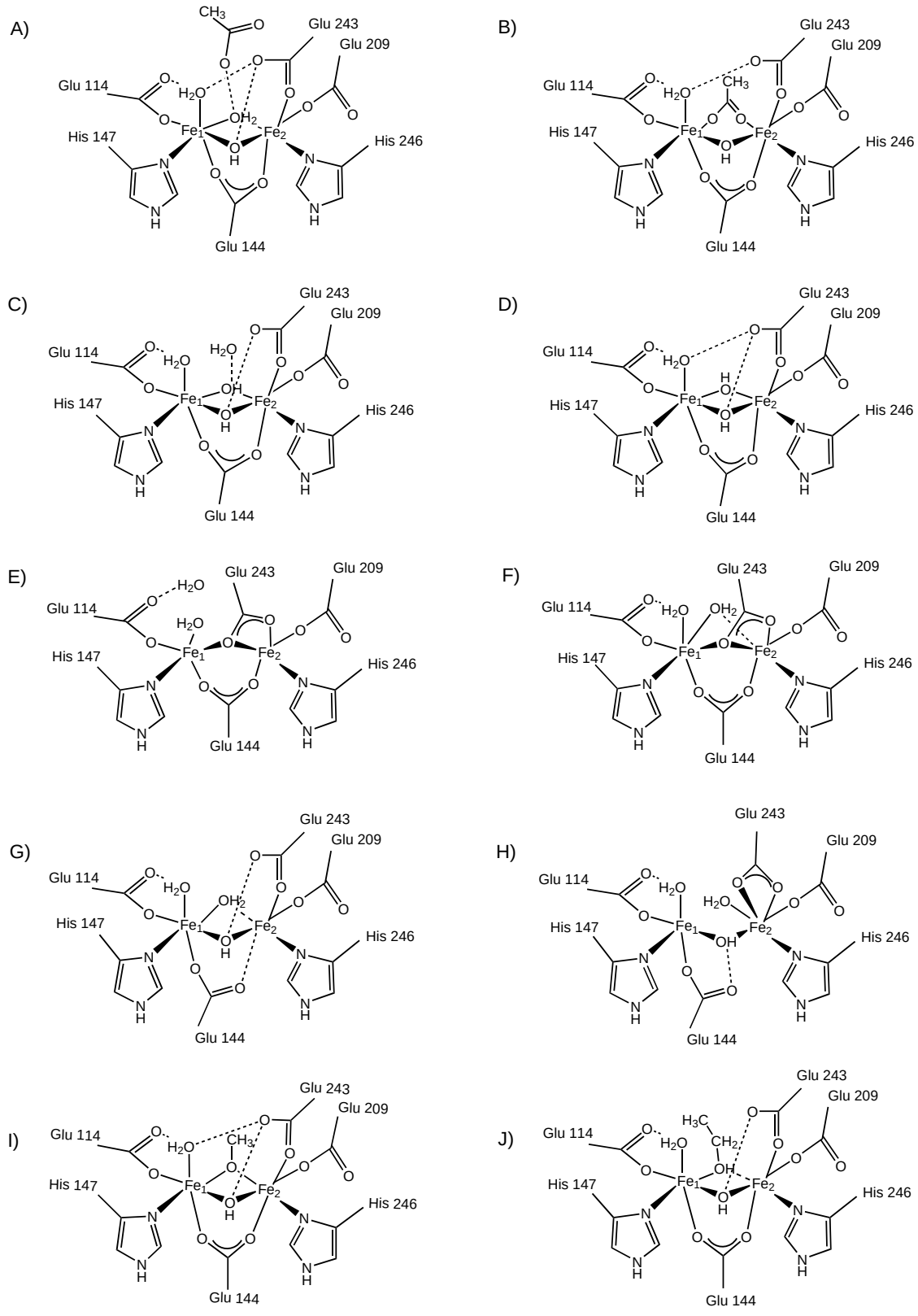

Figure 4. Coordination geometries for the diiron center of MMOH in various states: A) $MMOH_{ox}$, form I at 160 K; B) $MMOH_{ox}$, form I at 277 K; C) $MMOH_{ox}$, form II; D) $MMOH_{ox}$ from *M. trichosporium* OB3b, form I; E) $MMOH_{red}$, form I; F) $MMOH_{red}$, form II; G) $MMOH_{mv}$; H) $MMOH_{ox}$ soaked in 10% DMSO; I) $MMOH_{ox}$ soaked in 1M MeOH; J) $MMOH_{ox}$ soaked in 1M EtOH. All structures are for the enzyme from *M. capsulatus* (Bath), except (D) which is from *M. trichosporium* OB3b. The amino acid numbering for all structures is that of the enzyme from *M. capsulatus* (Bath). Dashed lines represent hydrogen bonds or very weak Fe–O interactions.

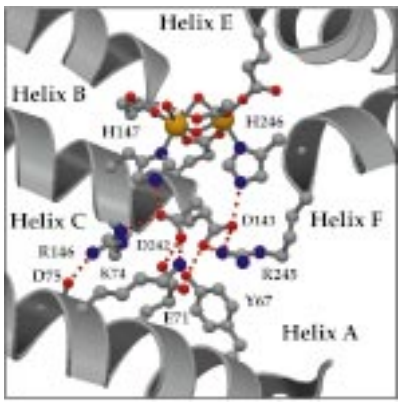

Figure 5. Structure of MMOH showing the hydrogen-bonding network of conserved residues that are proposed to be involved in electron transfer. The network extends from the two iron-coordinating histidines to the surface residues Tyr67 (Y67) and Lys74 (K74). This figure was produced with the programs Molscript and Raster3d.[232, 233] Reprinted with permission from ref. [234]. Copyright (2001) Wiley.

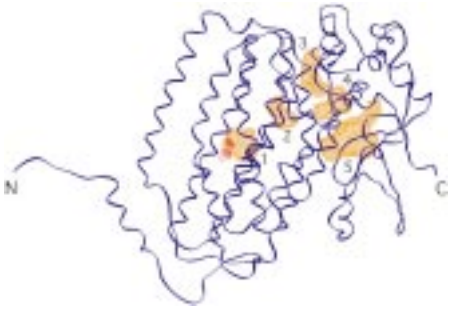

Figure 6. Ribbon diagram of MMOH α subunit showing five hydrophobic pockets that may be involved in substrate binding and transport to the active site. The figure was generated with the program O.[235] Reprinted with permission from ref. [122]. Copyright (1997) Wiley-Liss.

barrier between cavities 1 and 2, shifts from a "closed" to an "open" position upon reduction of MMOH in crystal form I (Figure 7). Only the opened rotamer is observed in the reduced and oxidized structures of form II MMOH from *M. capsulatus* (Bath), however.[33, 122] Another conserved residue that adopts different conformations is Asn214. The side chain of Asn214 points outward to the solvent in $MMOH_{ox}$, but is oriented inward toward the diiron site in all $MMOH_{red}$ structures.[33] This residue may therefore help to mediate the effects of MMOB on the redox properties of MMOH. Events such as reduction of the diiron center or binding of the other MMO components may control the conformation of Leu110 and other residues in order to "gate" the entry of substrate or solvent into the active site. Such a "leucine gate" was originally proposed to regulate access of O_2 to the diiron center in hemerythrin,[130, 131] but recent studies are more consistent with a role for Leu98 in gating access of solvent and not O_2.[132, 133]

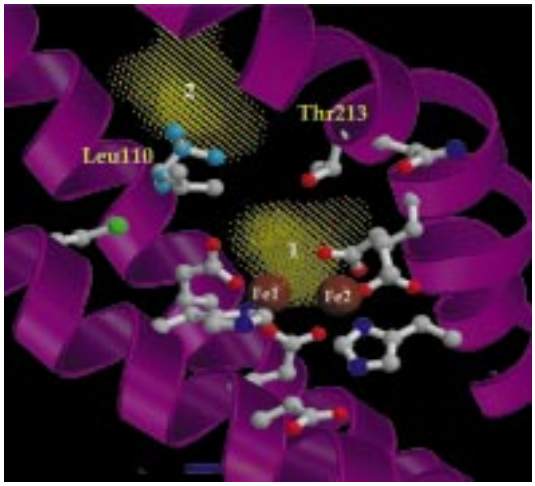

Figure 7. A closer look at the MMOH active site. Two conformations ("closed" in blue, "open" in gray) are depicted for Leu110, which may act as a gate that separates the hydrophobic cavities 1 and 2 (shown in yellow). This figure was produced with the programs Molscript and Raster3d.[232, 233]

2.2. MMOB

Addition of MMOB to the other sMMO components affects both the rate and the regioselectivity of hydroxylase-catalyzed reactions as well as the redox potentials of the MMOH diiron center (see Section 5 for additional discussion).[2, 24, 44–46, 48–50, 134] Similar effector proteins occur in other multicomponent monooxygenases such as toluene, phenol, and alkene monooxygenase.[54, 135] A variety of spectroscopic techniques suggest that MMOB exerts its effects on MMOH by binding in the vicinity of the diiron site and slightly altering its structure.[44, 46, 93, 98, 100, 108–110] Details of how the small, cofactorless MMOB protein regulates various aspects of MMO catalysis remain enigmatic. The recent elucidation of the three-dimensional structure of MMOB by NMR spectroscopy has yielded important geometric insights into the possible nature of the MMOH–MMOB interaction, however, and provides a good starting point for further studies of the mechanism of regulation by MMOB.

The structures of MMOB from both *M. capsulatus* (Bath) and *M. trichosporium* OB3b (Figure 8) have been solved by NMR spectroscopy, with average backbone root-mean square deviation (RMSD) values for the protein core of 0.46 Å and 1.1 Å, respectively.[31, 32] The core of MMOB, residues 35–127 in *M. capsulatus* (Bath), consists of seven β strands arranged into two antiparallel β sheets oriented almost perpendicular to each other (Figure 8A). Three α helices bridge the cleft

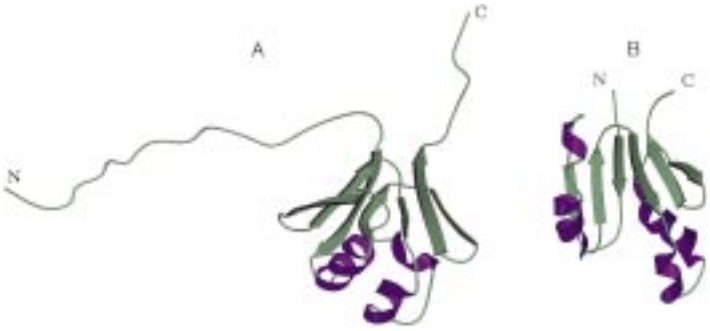

Figure 8. Ribbon diagrams of MMOB structures from A) *M. capsulatus* (Bath) (File in the protein data bank (PDB): 1CKV) and B) *M. trichosporium* OB3b (File in the PDB: 2MOB). This figure was produced with the programs Molscript and Raster3d.[232, 233]

between the two β sheets to create the globular core of the protein. The first 35 and the last 12 amino acids of MMOB are not well defined in the NMR structure, but NMR and CD experiments suggest that a part of the N terminus may form a helical structure.[31, 32, 83] Proteolytic cleavage in the N-terminal region completely inactivates MMOB.[83, 134, 136]

Structures have been determined by NMR spectroscopy for effector proteins of two other multicomponent hydroxylases, P2 in phenol hydroxylase from *Pseudomonas* sp. CF600 and T4moD in toluene-4-monooxygenase from *Pseudomonas mendocina*.[135, 137] The secondary structures of both effector proteins are similar to those found in MMOB, and the tertiary structure of T4moD is similar to that of MMOB from *M. capsulatus* (Bath) as well. Differences between MMOB and P2, which has a flatter structure with a "doughnut hole" in the center of the protein, may be explained by a lack of constraints in the latter structure, as indicated by a backbone RMSD of 2.48 Å. In addition, whereas NMR spectroscopy indicates that P2 interacts with substrate, such interactions have not been observed for MMOB.[31, 137]

NMR experiments with MMOB in the presence of the hydroxylase have identified several conserved surface residues that may be involved in binding to the larger hydroxylase protein.[32] Mapping those residues that show line-broadened NMR signals in the presence of MMOH onto the three-dimensional structure of MMOB indicates that most are located on the side of the protein that also contains the conserved residues E53, E94, L96, G97, F100, and D108 (Figure 9). Both the N and C termini extend from the other side of MMOB. In addition, NMR signals of a highly conserved region at the N terminus, residues 22 – 26, also experience line broadening at 25 °C. These results suggest that the lower half of MMOB is buried in some region of the hydroxylase, presumably the "canyon", whereas the upper half remains exposed to solvent. Interaction of the N terminus with surface residues of MMOH may explain the line broadening observed for residues 22 – 26.[28, 32, 33] This model is consistent with results from chemical cross-linking experiments that show MMOB interacting with the α subunit of MMOH.[44]

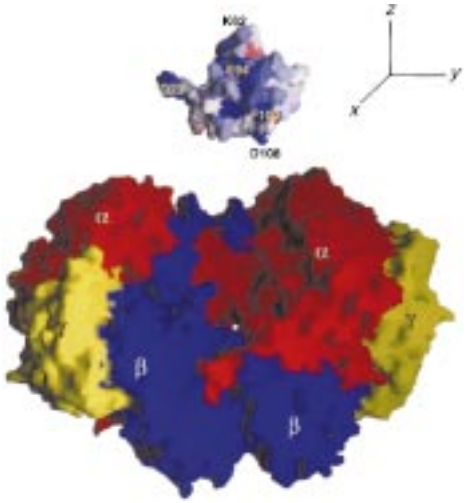

Figure 9. A surface diagram model for docking of MMOB (top) into the canyon of MMOH (bottom). Residues on MMOB that are most affected by binding to MMOH are colored blue and those least affected are colored red. For clarity, MMOB has been translated away from its proposed docking site on the surface of the hydroxylase and rotated clockwise about the y-axis by 90° to expose the residues on the "lower" half of MMOB most affected by MMOH binding. This figure was produced with the program Grasp.[236] Reprinted with permission from ref. [32]. Copyright (1999) National Academy of Sciences.

2.3. MMOR

MMOR is the one MMO component for which no three-dimensional structure has yet been determined. MMOR contains one [2Fe–2S] cluster and one FAD cofactor, which both facilitate electron transfer from NADH to MMOH.[24, 25, 27, 42, 43, 138, 139] In the absence of MMOH, the protein can transfer electrons from NADH to a variety of electron acceptors, including $K_3[Fe(CN)_6]$ and 2,6-dichloroindophenol (2,6-dichloro-*N*-(4-hydroxyphenyl)-1,4-benzoquinonimine), or it can reduce O_2 to hydrogen peroxide.[27, 138]

The [2Fe–2S] cluster is located in the N-terminal portion of MMOR and exhibits significant sequence homology with ferredoxins of plants, cyanobacteria, and archaebacteria.[53] Its optical,[27, 43] EPR,[43, 47, 138, 140] and Mössbauer[47] spectra are typical of those found for other [2Fe–2S]-type ferredoxins. The FAD cofactor is located in the C-terminal domain of MMOR, as is the NADH binding region. Upon one-electron reduction of the FAD cofactor, optical bands at 590 and 650 nm appear that are characteristic of a neutral semiquinone radical intermediate.[25, 27, 43, 84] The redox potentials of the MMOR cofactors are such that electron transfer in the physiological direction is favored: NADH ($E^{\circ\prime} = -320$ mV) → FAD ($E^{\circ\prime} = -266/-176$ mV) →[2Fe–2S] ($E^{\circ\prime} = -209$ mV) →MMOH ($E^{\circ\prime} \sim +100$ mV for ternary MMOH – MMOB – MMOR complex).[*][2, 42, 45, 84, 120, 140] The MMOR redox potentials are not significantly affected by the presence of MMOH or MMOB.[84]

In the absence of a high-resolution structure for MMOR, some structural insights may be gleaned from the X-ray diffraction results for related proteins, phthalate dioxygenase reductase (PDR) (Figure 10) and a complex between maize leaf [2Fe–2S] ferredoxin (Fd) and Fd–$NADP^+$ oxidoreductase (FNR).[141–143] Like MMOR, PDR shuttles electrons from NADH through flavin and [2Fe–2S] cofactors to an iron-containing oxygenase. The organization of the flavin and [2Fe–2S] domains is reversed, however, and PDR uses a flavin mononucleotide (FMN) instead of FAD.[141] In PDR, the [2Fe–2S]- and NADH-binding domains adopt the shape of a kidney bean, with the isoalloxazine group of FMN optimally positioned in the central cleft to mediate electron transfer from NADH to the [2Fe–2S] center. The distance between the closest Fe of the [2Fe–2S] center and the 8-methyl group of FMN is only 7.2 Å.

[*] The MMOR potentials listed are the ones most recently determined in our laboratory for the recombinant protein.[84] Similar values have been reported previously for native MMOR.[42, 140] All potentials are relative to the normal hydrogen electrode.

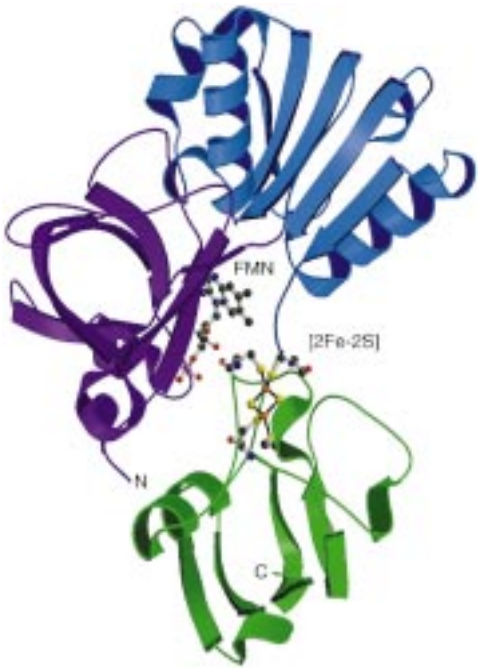

Figure 10. Ribbon diagram representation of the crystal structure of phthalate dioxygenase reductase showing the [2Fe–2S] and FMN cofactors in ball-and-stick representation (File in the PDB: 2PIA). The [2Fe–2S], FMN, and NADH-binding domains are colored in green, purple, and blue, respectively.[141] This figure was produced with the programs Molscript and Raster3d.[232, 233]

The complex between maize leaf [2Fe–2S] ferredoxin and Fd–NADP$^+$ oxidoreductase functions like MMOR and PDR, but the ferredoxin and flavin/NADP$^+$ binding parts are separate proteins instead of domains of the same protein. The overall folds of both proteins in this complex are similar to those of the corresponding domains in PDR, which indicates a common electron transfer pathway that is likely to exist in MMOR as well. One difference between the Fd–FNR complex and PDR is the orientation of the ferredoxin domain, which is rotated by about 180° around the axis from the closest Fe of the [2Fe–2S] center and the 8-methyl group of the flavin cofactor. It remains to be established which orientation is present in MMOR, but both result in approximately the same distance between the [2Fe–2S] center and the flavin cofactor.

3. Snapshots of the Catalytic Cycle

Knowing the three-dimensional structure of every intermediate on the enzymatic pathway is an enzymologist's ultimate dream, because it would allow a molecular movie to be compiled that illustrates how the enzyme works. The multicomponent nature of the MMO system makes the application of time-resolved crystallography difficult,[144] but time-resolved spectroscopic techniques have been remarkably successful in identifying and characterizing several intermediates in the catalytic cycle of MMO.[27, 50, 145–148] Two aspects of MMO catalysis have been studied by using time-resolved spectroscopy, the MMOR-promoted reduction of the diiron center by NADH and the dioxygen-activation and methane-hydroxylation steps at the MMOH diiron center.

3.1. Electron Transfer from NADH through MMOR to the Diiron Center in MMOH

Soluble methane monooxygenases employ a sophisticated electron transfer system with NADH-oxidizing and methane-hydroxylating sites on two separate proteins. This physical separation limits futile cycles whereby only NADH rather than NADH and methane are oxidized. Related systems can be found in bacterial monooxygenases, dioxygenases, and photosynthetic and respiratory electron transport chains.[3, 54, 149–151] Understanding all aspects of electron transfer within the MMO system and its regulation by component interactions may prove to be complex. Nonetheless, some intermediates of both the intramolecular (reduction of MMOR by NADH) and intermolecular (reduction of MMOH by MMOR) electron transfer steps have been identified by using stopped-flow optical spectroscopy.[27, 139]

Scheme 2 depicts intermediates that form during the reaction of MMOR$_{ox}$ with NADH.[27, 84] The first observable intermediate, termed CT1, is assigned as a charge-transfer complex between the nicotinamide moiety of NADH and the isoalloxazine ring of FAD. The rate of formation of CT1 becomes saturated as the concentration of NADH is increased, which indicates that NADH binding occurs in two steps. The initial Michaelis complex (MC1) is spectroscopically silent. A second charge-transfer intermediate, CT2, forms upon hydride transfer from NADH to FAD. CT2 has a more intense and lower energy absorbance band than CT1, because the π-stacking interaction now occurs between the NAD$^+$ cation and the FADH$^-$ anion. Release of NAD$^+$ and partial electron transfer from FADH$^-$ to [2Fe–2S]$_{ox}$ are observed to occur simultaneously. This single-electron transfer step yields a flavin semiquinone and [2Fe–2S]$_{red}$.

When NADH is mixed with a 1:1 complex of MMOH$_{ox}$ and MMOR$_{ox}$, the early steps of NADH binding to MMOR and hydride transfer are largely unchanged.[27] NAD$^+$ release and electron transfer from FADH$^-$ proceed at rates similar to those seen for MMOR alone, although this state comprises a mixture of complexes with two electrons in MMOR and complexes with one electron in MMOR and the other

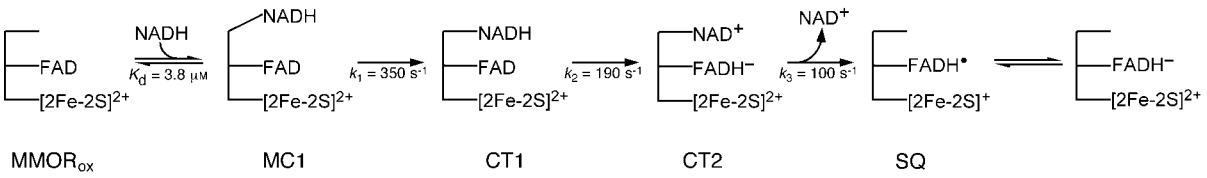

Scheme 2. Intermediates formed upon reaction of MMOR$_{ox}$ with NADH.

electron in MMOH. Further electron-transfer steps to MMOH, ultimately to afford $MMOH_{red}$, proceed at slower rates. Addition of MMOB increases the rate of these intermolecular electron-transfer reactions, with maximum rates observed when one equivalent of MMOB is present per MMOH. Methanol retards intermolecular electron transfer, whereas methane has no effect.

The presence of additional electron-transfer steps occurring among cofactors of MMOR complicates the spectral analysis for the intermolecular electron-transfer reaction. Studies using prereduced MMOR or studies using just the N-terminal ferredoxin-like domain of MMOR should resolve this problem and allow a better understanding of intermolecular electron transfer from MMOR to MMOH.[152]

3.2. Transient Intermediates in the Activation of O_2

Methane monooxygenase has proved to be a rewarding system for studying the molecular details of dioxygen activation at a non-heme diiron center. Two critical properties of sMMO are responsible for this success. First, chemically reduced MMOH can react with O_2 and substrate to afford hydroxylated products and $MMOH_{ox}$ in the absence of the other MMO components.[24] Although the yields for this single-turnover reaction are variable and below 40%, this result nonetheless proves that activation of dioxygen and the actual hydroxylation reaction both take place at the MMOH protein.[24, 50] Even more important is that, in the presence of MMOB, the energetics of the reaction pathway are such that several intermediates build up in significant amounts before they decay.

Figure 11 displays species in the catalytic cycle that have been detected during the single-turnover reaction of $MMOH_{red}$ with O_2 in the absence and presence of substrate.[50, 145, 147, 148] The reaction can be monitored continuously by using stopped-flow optical spectroscopy to detect colored intermediates or discontinuously by using the freeze–quench method in combination with EPR, Mössbauer, and EXAFS spectroscopy. The decay of $MMOH_{red}$ has been followed by EPR (decay of the $g = 16$ signal) and Mössbauer spectroscopy.[49, 50, 120, 145] In the presence of MMOB, the $g = 16$ signal of $MMOH_{red}$ from *M. trichosporium* OB3b decays at a rate of $22 \pm 5\ s^{-1}$ at 4 °C. No new EPR signals appear on this time scale.[145] The decay of $MMOH_{red}$ is independent of the dioxygen concentration between 0.3 and 0.7 mM, which indicates the formation of a transient Michaelis complex between $MMOH_{red}$ and O_2 prior to the decay of the $g = 16$ signal. No such complex forms between $MMOH_{ox}$ and O_2, however.[153] A fact that is not often mentioned in reviews and discussions on the mechanism of dioxygen activation by MMOH is that a substantial portion of $MMOH_{red}$ seems to be inactive and is converted into $MMOH_{ox}$ on a timescale that is too slow to be catalytically relevant.[50, 95, 146, 147, 154, 155] The presence of these two populations of $MMOH_{red}$ is a complicating factor in the spectroscopic characterization of intermediates.

The first intermediate that is observed spectroscopically following the decay of $MMOH_{red}$ is $MMOH_{peroxo}$. First

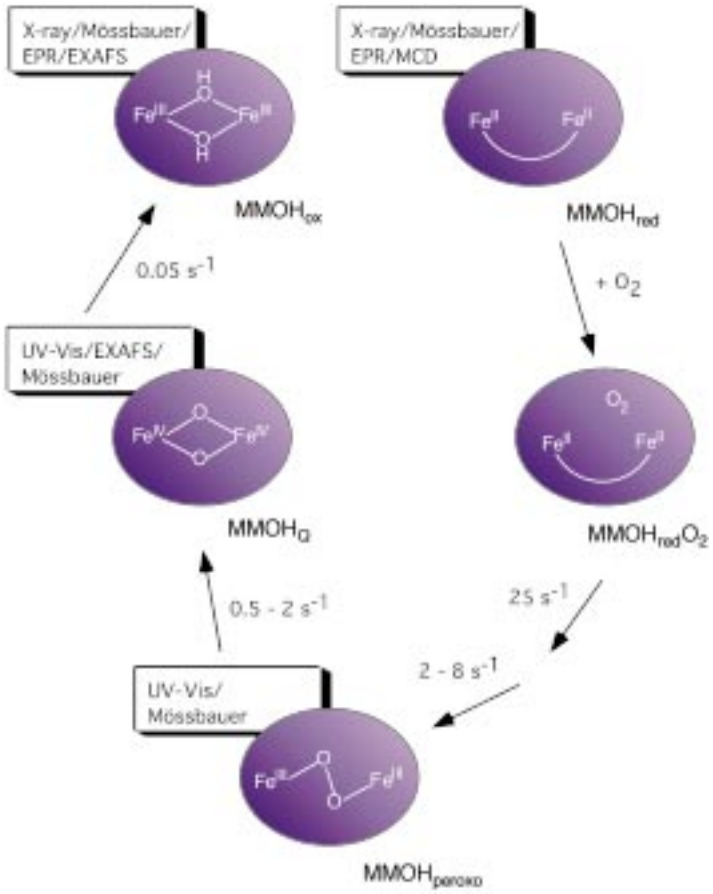

Figure 11. Schematic overview of the catalytic intermediates observed for the single turnover reaction of $MMOH_{red}$ with O_2. Techniques used to characterize the various intermediates are indicated. Structures other than those shown here have been proposed for the $MMOH_{peroxo}$ and $MMOH_Q$ intermediates. The rate constants are from studies of both the *M. capsulatus* (Bath) and the *M. trichosporium* OB3b enzymes and were determined in MOPS buffer (MOPS = 3-(*N*-morpholino)propanesulfonic acid; pH 7.0) at 4 °C.

detected for *M. capsulatus* (Bath), $MMOH_{peroxo}$ has optical bands at 420 ($\varepsilon = 4000\ M^{-1}cm^{-1}$) and 725 nm ($\varepsilon = 1800\ M^{-1}cm^{-1}$).[50, 147, 154, 155] A similar intermediate has recently been reported for the enzyme from *M. trichosporium* OB3b with $\lambda_{max} = 700$ nm ($\varepsilon = 2500\ M^{-1}cm^{-1}$),[156] although the intensity of the absorption band at 420 nm may be lower.[157] The Mössbauer spectrum of $MMOH_{peroxo}$ consists of a sharp quadrupole doublet with $\delta = 0.66\ mm\,s^{-1}$ and $\Delta E_Q = 1.51\ mm\,s^{-1}$, which is consistent with two high-spin iron(III) centers having a similar coordination geometry.[50, 154] $MMOH_{peroxo}$ is diamagnetic at 4 K as a result of antiferromagnetic coupling between the two Fe^{III} ions. Intermediates with similar optical and Mössbauer properties have been detected in a number of other diiron proteins that activate O_2, including stearoyl-ACP Δ^9 desaturase, the D84E mutant of the R2 protein of class I ribonucleotide reductase, and frog ferritin. No reliable resonance Raman data have yet been obtained for $MMOH_{peroxo}$,[155, 158] although resonance Raman spectroscopy has identified all of the other peroxo intermediates as μ-1,2-peroxo diiron(III) complexes. Table 3 compares the spectroscopic properties of these species with those of a structurally characterized μ-peroxo diiron(III) model complex.

Table 3. Spectroscopic properties of peroxo-bridged diiron(III) centers in proteins and a model complex.

	Vis		Resonance Raman		Mössbauer (4.2 K)	
	λ_{max} [nm]	ε [$M^{-1}cm^{-1}$]	O–O [cm^{-1}]	Fe–O [cm^{-1}]	δ [$mm\,s^{-1}$]	ΔE_Q [$mm\,s^{-1}$]
MMO (*M. caps.*)	700	1800[147]	–	–	0.66	1.51[50, 154]
MMO (*M. trich.*)	725	2500[156]	–	–	0.67	1.51[95]
R2-D84E	700	1500[225]	890[39]	–	0.63	1.58[225]
R2-D84E/W48F[226]	700	–	870	458	–	–
Δ^9 desaturase	700	1200[227, 228]	898	442[227]	0.68	1.90
					0.64	1.06[228]
frog M ferritin	650[229]	–	851	485(s) 499(as)[230]	0.62	1.08[229]
cis-μ-1,2-peroxo Fe_2^{III}	694	2650[159]	888[159]	–	0.66	1.40[159]

This diiron(III) synthetic model with optical and Mössbauer properties that are very similar to those of $MMOH_{peroxo}$ was structurally characterized and shown to contain a *cis*-μ-1,2 peroxo group.[159] The peroxo intermediate found for frog M ferritin is the only one thus far characterized by EXAFS spectroscopy.[160] A surprisingly short Fe–Fe distance of 2.53 Å, compared to the value of 4.004 Å in the synthetic model complex,[159] implies the presence of two single-atom bridges in addition to the μ-1,2 peroxo bridge. The structure of the ferritin peroxo intermediate is not necessarily similar to peroxo intermediates in other diiron proteins, however. Ferritin is the only protein listed in Table 3 that is not involved in the oxidation of organic substrates. Its peroxo intermediate also has somewhat lower values for λ_{max} (650 nm), ΔE_Q (1.06 $mm\,s^{-1}$), and the O–O stretching frequency (851 cm^{-1}) than those of the other diiron proteins.

Although time-resolved optical and Mössbauer studies were initially interpreted with a model in which a single peroxo intermediate forms directly from $MMOH_{red}$ and O_2, more recent stopped-flow optical studies on enzymes from both *M. capsulatus* (Bath) and *M. trichosporium* OB3b have provided evidence for the formation of one or more species preceding $MMOH_{peroxo}$. The rates for formation and decay of $MMOH_{peroxo}$ from the latter organism are pH dependent, both being faster at low pH values.[156] A single pK_a value of 7.6 was reported for both reactions. The formation rate of $MMOH_{peroxo}$ is significantly lower than the decay rate of the $g = 16$ EPR signal of $MMOH_{red}$, and the decay of the $g = 16$ signal is pH independent. Both observations can be explained by the presence of an intermediate that lacks both the $g = 16$ EPR signal and the optical characteristics of $MMOH_{peroxo}$. Recently, it was shown that a model incorporating a species between $MMOH_{red}$ and $MMOH_{peroxo}$ (named P*) better describes the absorbance changes, especially at early time points.[157] The formation rate of P* is equal to the decay rate of $MMOH_{red}$ as determined by EPR spectroscopy, whereas its decay rate corresponds to the formation rate of $MMOH_{peroxo}$. Recent stopped-flow optical studies on *M. capsulatus* (Bath) MMOH found a formation rate constant for $MMOH_{peroxo}$ of only 1–2 s^{-1} at 4 °C, which is lower than that of 25 s^{-1} which was originally reported.[147] This result was also interpreted as indicative of the presence of an intermediate preceding $MMOH_{peroxo}$, which could be a different peroxo species or a superoxo complex. In contrast to the *M. trichosporium* OB3b enzyme, formation and decay of $MMOH_{peroxo}$ is pH independent for the enzyme from *M. capsulatus* (Bath).[50]

A different approach to probe the nature of early steps in the activation of dioxygen is to measure the oxygen kinetic isotope effect (KIE) for MMO catalysis. A KIE of 1.016 ($v/K(^{16}O^{16}O)/v/K(^{18}O^{16}O)$, v = velocity, K = Michaelis constant) was obtained for the enzyme from *M. capsulatus* (Bath), both in the presence and absence of acetonitrile as the substrate.[153] A KIE of 1.016 indicates a significant decrease in O–O bond order up to the first irreversible step in the activation of dioxygen and argues against the formation of a tight, irreversible $MMOH_{red}$–O_2 complex. The magnitude of the KIE is consistent with one-electron reduction of O_2 to superoxide as the first irreversible step in dioxygen activation. Other possibilities cannot be ruled out, however. Formation of a superoxide species has also been proposed to be the first irreversible step in the reductive activation of dioxygen in a number of other oxygen-activating metalloenzymes.[161, 162]

Most peroxo complexes prepared as synthetic models are stable only at low temperature and tend to decay directly to form diferric species.[1, 163–165] In contrast, the protein matrix surrounding the diiron center in MMOH allows $MMOH_{peroxo}$ to be converted into a high-valent oxo intermediate, termed $MMOH_Q$. Formation and decay of $MMOH_Q$ can be monitored conveniently by stopped-flow spectroscopy due to its bright yellow color ($\varepsilon_{350nm} = 3600\,M^{-1}cm^{-1}$; $\varepsilon_{420nm} = 7200\,M^{-1}cm^{-1}$).[50, 145–147, 154, 157] In the absence of substrate, $MMOH_Q$ decays slowly (approximately 0.05 s^{-1}) to form $MMOH_{ox}$. Unlike the decay of $MMOH_{peroxo}$, which is not affected by the presence of most substrates (see Section 4 for an important exception), the decay rate of $MMOH_Q$ increases in the presence of hydrocarbon substrates.[50, 145, 147, 157] This observation identifies $MMOH_Q$ as the active oxygen intermediate that reacts with methane and other substrates. For methane and most other substrates, the decay rate of $MMOH_Q$ depends linearly on the substrate concentration, which suggests that substrates are not tightly bound in the active site.[50, 145, 147, 157] The Eyring plot for $MMOH_Q$ decay in the presence of methane is linear for *M. capsulatus* (Bath), but nonlinear behavior has been reported recently for the enzyme from *M. trichosporium* OB3b. Curiously, the latter result was interpreted by a two-step model for $MMOH_Q$ decay in which the rate-limiting step changes from C–H bond scission at low temperatures to substrate binding at high temperatures.[157] No intermediates have been identified in the reaction of $MMOH_Q$ with methane and other hydrocarbon substrates. Only for nitrobenzene has formation of a distinct product

complex been spectroscopically observed.[50, 145] For this substrate, product release from the hydrophobic active site can be observed because of the distinct color difference between the protonated *p*-nitrophenol in the hydrophobic active site and the deprotonated *p*-nitrophenolate ion in the bulk solution. In this particular case, the rate of product release is similar to the turnover rate from steady-state measurements, consistent with product release being the rate-limiting step in the oxygenation of nitrobenzene.

Characterization of $MMOH_Q$ by rapid freeze–quench (RFQ) Mössbauer spectroscopy revealed that both iron atoms have isomer shifts that are significantly smaller than those typical of diiron(III) complexes and more consistent with a diiron(IV) assignment.[50, 146] The sharp quadrupole doublet observed for the *M. trichosporium* OB3b enzyme ($\delta = 0.17\ mm\,s^{-1}$ and $\Delta E_Q = 0.53\ mm\,s$) suggests similar ligand environments for both iron atoms, whereas two slightly different iron environments were detected for the *M. capsulatus* (Bath) enzyme (Fe 1: $\delta = 0.21\ mm\,s^{-1}$, $\Delta E_Q = 0.68\ mm\,s^{-1}$; Fe 2: $\delta = 0.14\ mm\,s^{-1}$, $\Delta E_Q = 0.55\ mm\,s^{-1}$). The absence of splitting in these quadrupole doublets at high applied magnetic field strongly supports the formulation of $MMOH_Q$ as a diiron(IV) cluster having a diamagnetic ground state due to antiferromagnetic coupling between the iron atoms.

Important structural information has also been obtained from analysis of the EXAFS spectra of RFQ samples containing high amounts (40–60%) of $MMOH_Q$.[95] A very short Fe–Fe distance of 2.46 Å was reported, together with one short (1.77 Å) and one long (2.0 Å) Fe–O bond. The short Fe–Fe distance strongly indicates the presence of at least two single oxygen bridges. An additional carboxylate bridge was proposed to explain the short Fe–Fe distance in $MMOH_Q$ compared to model complexes with similar structures. An EXAFS analysis of the enzyme from *M. capsulatus* (Bath) supports the presence of a short Fe–Fe distance in $MMOH_Q$.[166]

An important mechanistic question is whether the O–O bond in $MMOH_{peroxo}$ is cleaved homolytically or heterolytically to form $MMOH_Q$. Figure 12 depicts two possibilities for the conversion of $MMOH_{peroxo}$ into $MMOH_Q$. In the heterolytic mechanism, a monodentate peroxo complex may form in

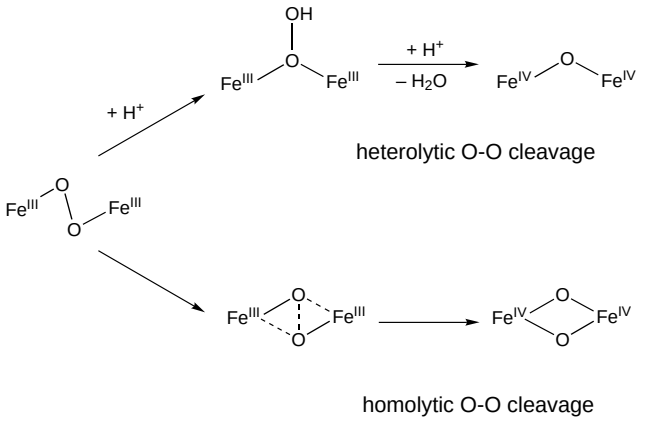

Figure 12. Comparison of the heterolytic and homolytic cleavage mechanisms for the conversion of $MMOH_{peroxo}$ into $MMOH_Q$.

which one of the oxygen atoms is protonated. Addition of a second proton to this oxygen facilitates heterolytic cleavage of the O–O bond and formation of a high-valent diiron complex in which one of the dioxygen-derived oxygen atoms forms an oxo bridge, while the other is released as water. This mechanism resembles those proposed for the P450 monooxygenases and heme-containing peroxidases, in which protonation of a ferric hydroperoxo complex also results in heterolytic O–O bond cleavage and the release of water. The oxidation state in the $Fe^{IV}{=}O(P^{\bullet+})$ intermediate (compound I, where P = porphyrin) that is believed to be formed in this step is equivalent to that in $MMOH_Q$. In the heme-containing enzymes, oxidizing equivalents are stored on both the iron and the porphyrin ring, whereas the same oxidation state is reached in MMO by oxidizing two iron atoms to the +4 level. The pH dependence observed for the formation and the decay of $MMOH_{peroxo}$ for the M. *trichosporium* OB3b enzyme is consistent with such a mechanism.[156] The linear proton inventory plots reported in the same study imply transfer of a single proton in the transition states of both reactions. Finally, the formation of $MMOH_Q$ shows a positive entropy change, which could be due to release of water.[50, 147]

A fundamentally different mechanism is one in which the O–O bond is cleaved homolytically resulting in a bis(μ-oxo)diiron(IV) species. Oxygen–oxygen bond cleavage by dicopper centers is believed to proceed by such a mechanism.[167–169] In this case, both dioxygen-derived oxygen atoms become bridging oxide ligands of the diiron center, and water is released in some step following the decay of $MMOH_Q$.

Distinguishing between these mechanistic possibilities would benefit from more detailed knowledge of the $MMOH_Q$ structure. Although EXAFS spectroscopy indicates the presence of at least two single-atom bridges, it cannot distinguish between two oxo bridges, a structure that is most easily explained by homolytic cleavage of the O–O bond in $MMOH_{peroxo}$, and a structure with one oxo and one or more single-oxygen glutamate bridges. The latter structure would support heterolytic cleavage of the O–O bond. The EXAFS spectrum of $MMOH_Q$ is remarkably similar to that of intermediate X, a high-valent intermediate that is formed transiently during the reaction of the diferrous R2 protein of ribonucleotide reductase with O_2.[170] Like $MMOH_Q$, intermediate X has a short Fe–Fe distance of 2.5 Å, and thus a structure with at least two single-atom bridges. In contrast to $MMOH_Q$, intermediate X is best described as a mixed-valent $Fe^{III}Fe^{IV}$ species.[171] Antiferromagnetic coupling between Fe^{III} and Fe^{IV} gives rise to an $S = 1/2$ ground state, which has allowed its structure to be characterized thoroughly by using EPR and ENDOR spectroscopy.[172] Labeling studies using $^{17}O_2$ and $H_2{}^{17}O$ show that one of the oxygen atoms of the O_2 molecule forms an oxo bridge, while the other oxygen atom forms a terminal aqua ligand to Fe^{III}.[172, 173] This result in turn implies that one of the single-atom bridges in intermediate X is provided by a carboxylate ligand.

To probe further the relationship between the structures of intermediate X and $MMOH_Q$, we recently employed radiolytic reduction at 77 K to produce a one-electron reduced form of $MMOH_Q$ (called $MMOH_{Q_X}$). $MMOH_{Q_X}$ is expected to

retain the structure of $MMOH_Q$, because of the low temperature at which it is generated.[174] The Mössbauer parameters of $MMOH_{Qx}$ are remarkably similar to those reported for intermediate X: Fe1: $\delta = 0.48\ mm\,s^{-1}$, $\Delta E_Q = -0.9\ mm\,s^{-1}$; Fe2: $\delta = 0.14\ mm\,s^{-1}$, $\Delta E_Q = -0.6\ mm\,s^{-1}$.[171] EPR/ENDOR studies on $MMOH_{Qx}$ similar to the ones done on intermediate X with $^{17}O_2$ and $H_2{}^{17}O$ could help to distinguish between the homolytic and heterolytic O–O bond cleavage mechanisms. Such studies are difficult because of the presence of intense EPR signals from free radicals that are generated by the high-energy γ-rays used for radiolytic reduction.

Recently several groups have applied DFT to calculate the MMO catalytic pathway.[175–184] DFT calculations can afford insights into reasonable structures for the spectroscopically detected oxygen intermediates and suggest species that have remained undetected so far. In addition, they provide a powerful tool to probe the nature of the reaction between $MMOH_Q$ and substrates (see Section 4). MMO is especially amenable to the DFT approach because most of the important chemistry involving dioxygen activation and substrate oxygenation occurs at the diiron center. Models with a relatively small number of atoms may therefore describe the active site satisfactorily.

The most extensive DFT study reported thus far uses a model based on approximately 100 atoms.[182] Such a relatively large model was required for these calculations to reproduce faithfully the structures of $MMOH_{ox}$ and $MMOH_{red}$, both known from X-ray crystallography. Figure 13 provides a "DFT view" of the catalytic cycle of MMO from this work, and shows those structures for $MMOH_{superoxo}$, $MMOH_{peroxo}$, and $MMOH_Q$ intermediates having the lowest energy. A remarkable finding of these calculations is the suggestion that a coordinated water remains ligated to Fe1 in a terminal position throughout the catalytic cycle. The energies of the superoxo and peroxo complexes are comparable. The asymmetric nature of $MMOH_{peroxo}$ is somewhat surprising in view of the sharp quadrupole doublet observed in the Mössbauer spectrum of this intermediate. A recent DFT study that used a smaller model of 40 atoms suggests a slightly more stable, symmetric μ-η^2:η^2 nonplanar (butterfly) peroxo structure as an alternative for the $MMOH_{peroxo}$ structure depicted in Figure 13 (see also below).[184]

The DFT structure of $MMOH_Q$ is reasonably consistent with spectroscopic data, including the presence of a short Fe–Fe distance of 2.67 Å and an antiferromagnetically coupled spin state. In contrast to the EXAFS study that

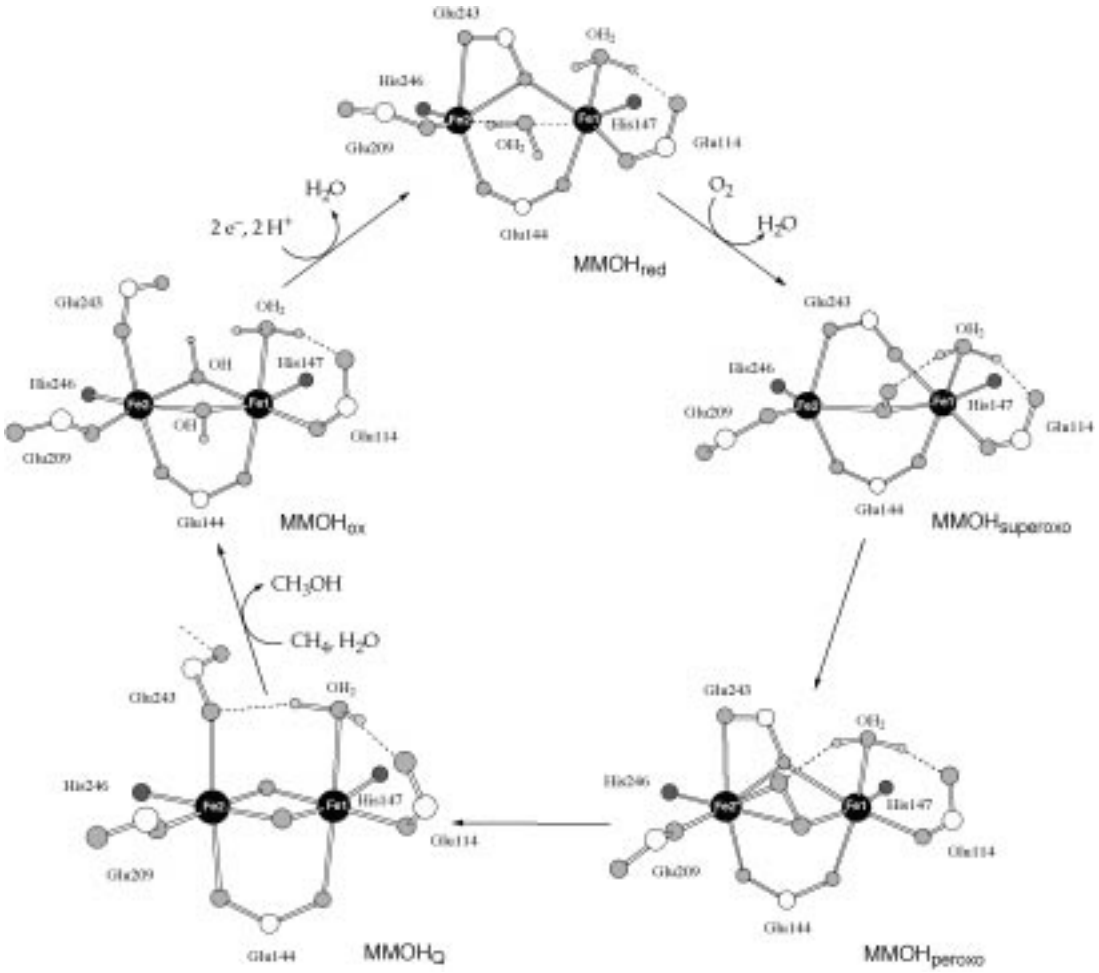

Figure 13. A "DFT view" of the catalytic cycle of MMO. Note that the positions of Fe1 and Fe2 are reversed compared to other figures in this paper, to allow a better view of the dioxygen activation reaction. Adapted with permission from ref. [182]. Copyright (2000) American Chemical Society.

reported the presence of one short (1.77 Å) and one long (2.0 Å) Fe–O bond, however, the DFT structure of $MMOH_Q$ shows more symmetrically bridging oxo groups, as reflected in Fe–O bond distances of 1.76 and 1.81 Å. The recent DFT study that used a smaller set of 40 atoms confirmed that this $MMOH_Q$ structure, with one bridging carboxylate and one water directly coordinated to one of the iron atoms, is significantly more stable than the structures with two bridging carboxylates found in earlier DFT calculations.[184] The same study also investigated the mechanism of O–O bond cleavage in the conversion of $MMOH_{peroxo}$ into $MMOH_Q$. A homolytic mechanism was proposed starting from a μ-η^2:η^2 nonplanar (butterfly) $MMOH_{peroxo}$ structure. Only one of the iron atoms was invoked as being actively involved in the cleavage reaction. DFT calculations using the 100-atom model confirm the existence of this μ-η^2:η^2 peroxo structure in the transition from $MMOH_{peroxo}$ into $MMOH_Q$.[185] Additional DFT calculations are required to clarify further the nature of this and other steps in the dioxygen activation reaction.

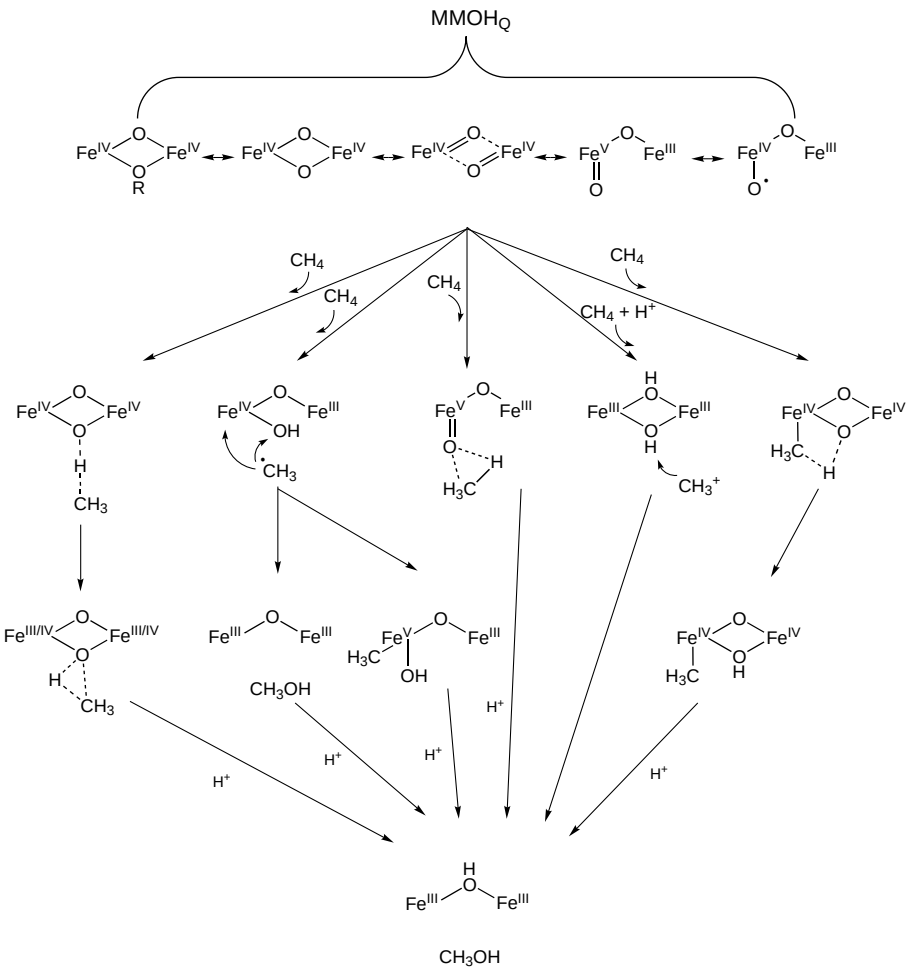

Figure 14. Some of the mechanisms proposed for hydroxylation of methane by $MMOH_Q$.

4. Mechanism of Hydrocarbon Hydroxylation

The spectroscopic studies of transient species described in the preceding section have yielded key insights into the nature of intermediates involved in dioxygen activation and have identified $MMOH_Q$ as the intermediate that reacts with methane and other hydrocarbons. The next question is to understand how $MMOH_Q$ hydroxylates substrate molecules. Since no intermediates have been observed for this step by using rapid-mixing spectroscopic methods, more indirect methods have been applied. Substrate probes have helped to delineate the chemical characteristics of the hydroxylation steps, and theoretical studies have been employed to probe the mechanistic details.

Mechanistic proposals for the hydroxylation of the C–H bond have been thoroughly reviewed.[1, 3, 5, 186–192] The possibilities depicted in Figure 14 illustrate some of the important issues: What is the structure of $MMOH_Q$ that reacts with methane? Is the reactive species best formulated as a bis(μ-oxo)diiron(IV) moiety, as proposed by EXAFS studies, or as an Fe^{III}–O–Fe^{V}=O species? Are the iron atoms coordinatively saturated, or are they five-coordinate, to allow the formation of Fe–C bonds? Are (short-lived) substrate radicals involved, in a mechanism that is similar to the widely cited oxygen-rebound mechanism proposed for cytochrome P450 monooxygenases? Or is hydroxylation better described by a concerted mechanism in which an activated oxygen atom inserts directly into a C–H bond?

Most of the experimental approaches that can distinguish between these mechanistic proposals rely on the use of reporter substrates, molecules that yield different products depending on the type of reaction they undergo. MMO has a broad substrate selectivity, and many different compounds have been used in such studies. One method is to investigate alkane substrates made chiral by isotopic substitution. Concerted mechanisms would predict either complete retention or complete inversion of stereochemistry at the hydroxylated carbon atom, whereas the formation of radical or carbocation intermediates should result in full racemization. Hydroxylation of (*R*)- or (*S*)-[1-^{2}H,1-^{3}H]ethane occurs predominantly (64–74%) with retention of configuration for both *M. capsulatus* (Bath) and *M. trichosporium* OB3b,[186, 193] and with approximately 90% retention for [2-^{3}H]butane.[193] Initially, the observation of a measurable amount of racemization was taken as evidence for a radical-based intermediate species.[186] Others pointed out, however, that 70% retention corresponds to a rebound rate for the putative ethyl radical of

1×10^{13} s^{-1}.[193] Such a large rate constant is inconsistent with the formation solely of a discrete radical intermediate.

A substantial amount of work has been devoted to the use of radical-clock substrate probes.[194–196] These compounds undergo rearrangement of their carbon skeletons following hydrogen-atom abstraction. Because rate constants for such rearrangements have been experimentally determined, analysis of product ratios from MMO-catalyzed hydroxylation allows calculation of lifetimes for any substrate radical species. The vast majority of the radical-clock substrates tested with the *M. capsulatus* (Bath) enzyme yield only unrearranged products; this finding argues against discrete radical species occurring during MMO catalysis.[197, 198] From a series of cyclopropane-based radical-clock substrates that were studied for the *M. trichosporium* OB3b enzyme, most again showed no rearranged products.[199] Such results place an upper limit of 150 fs on the lifetime for a radical species, too short to account for the formation of a discrete radical intermediate.

Rearranged products have been reported for four specific substrates, however, all of which can discriminate between radical- and carbocation-type rearrangements.[199–203] The three best-studied cases are depicted in Figure 15. Oxidation of 1,1-dimethylcyclopropane gives mostly the unrearranged product (1-methylcyclopropyl)methanol, but also small amounts of the radical-type rearrangement product (3-methyl-3-buten-1-ol, 6%) and the carbocation-type product (1-methylcyclobutanol, 13%).[200] Similar results were obtained by using (*trans,trans*-2-methoxy-3-phenylcyclopropyl)-methane as the substrate,[202] and the carbocation-type product 1-homocubanol was obtained as the major product from the oxygenation of methylcubane.[201–203]

An alternative method to test for the involvement of radical intermediates is applying spin traps. Steady-state oxidation of methane, methanol, and acetonitrile in the presence of such spin traps and subsequent analysis by EPR spectroscopy showed the formation of adducts with substrate radicals.[204, 205] It is difficult to assess whether these species are due to some minor formation of radicals or represent true catalytic intermediates, however.

Studies of the $^1H/^2H$ kinetic isotope effect can provide information about the nature of a transition state in which the C–H bond is broken. Large kinetic isotope effects have been correlated with a linear O–H–C geometry and substantial C–H bond cleavage in the transition state.[206, 207] The series CH_4, CH_3D, CH_2D_2, CHD_3, and CD_4 was investigated to probe kinetic isotope effects for the MMO enzyme from *M. trichosporium* OB3b. Both the rate of $MMOH_Q$ decay and product ratios were analyzed.[208] A surprisingly large isotope effect of 50–100 was found for $MMOH_Q$ decay for CH_4 versus CD_4, whereas a significantly smaller but still large value of 28 was reported for *M. capsulatus* (Bath).[147] For *M. trichosporium* OB3b no kinetic isotope effects were observed for $MMOH_Q$ decay using larger substrates (C_2H_6 versus C_2D_6 and C_3H_8 versus C_3D_8), however, which was rationalized by assuming that a substrate-binding step determines the rate of $MMOH_Q$ decay for these substrates rather than C–H bond breakage.[157] A similar lack of kinetic isotope effect for ethane has been observed for *M. capsulatus* (Bath).[209]

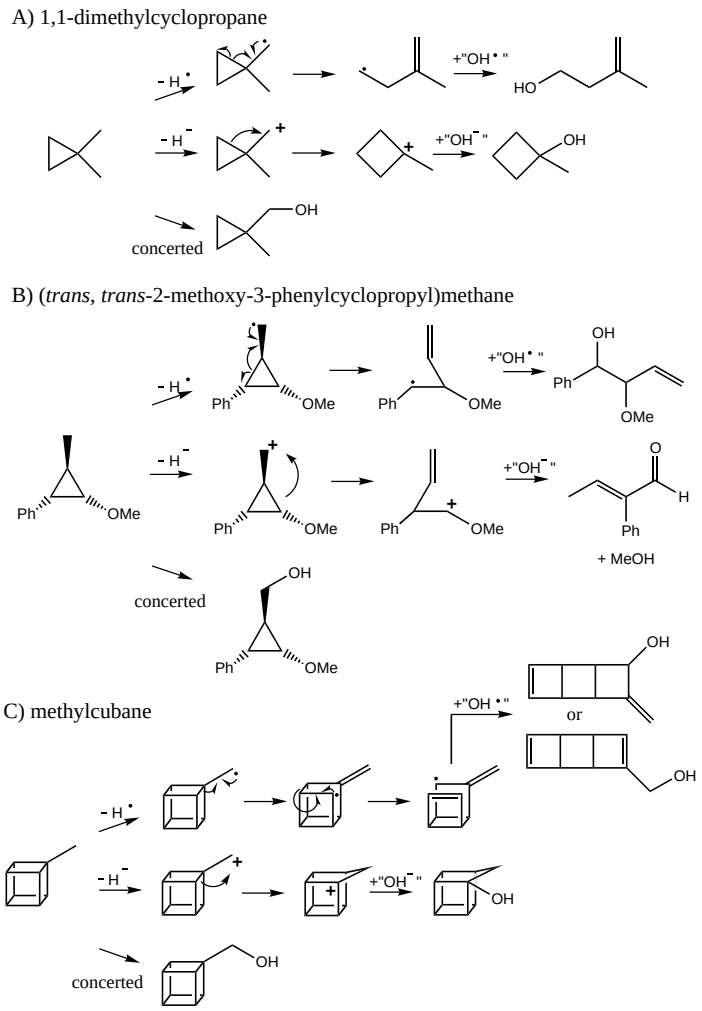

Figure 15. Three substrates that react differently depending on the type of hydroxylation reaction (radical intermediate, carbocation intermediate, or concerted). Products from more than one type of reaction have been observed with all three substrates.

Intramolecular kinetic isotope effects for methane obtained by studying product ratios yield smaller values, which also depend on the specific methane isotopomer (19.3 for CH_4 versus CD_4, but only 3.9 for the intramolecular effect in CD_3H). Experiments using chiral ethane gave intramolecular isotope effects in the range of 3–4.[186, 193] For comparison, typical k_H/k_D values of 7–10 were reported for P450 hydroxylation.[34] The reaction of CD_4 with $^{18}O_2$ results in 100% $CD_3{}^{18}OH$, and shows no exchange of oxygen or methyl hydrogen atoms with the solvent.[208] Hydrogen tunneling was proposed as the most likely reason for the large isotope effect on $MMOH_Q$ decay. The discrepancies between the different KIEs indicate the presence of a complex mechanism of $MMOH_Q$ decay, and/or substrate oxidation by pathways other than $MMOH_Q$ decay.

Several theoretical studies have been employed to probe the mechanism of the hydroxylation reaction, most of them using DFT methods (see also Section 3). Initially a simple model was investigated for $MMOH_Q$ involving a bis(μ-oxo)-diiron(IV) core with a bridging formate and terminal hydroxo and water ligands.[210] In this model, which has an all-oxygen

atom donor set, the most stable configuration has five-coordinate iron atoms. $MMOH_Q$ abstracts a hydrogen atom from methane to give an $Fe^{III}(\mu\text{-}O)(\mu\text{-}OH)Fe^{IV}$ species with an iron-bound methyl group, although the precise outcome of the reaction depends on the spin state assigned to the starting iron complex. Later work using a larger model, a bis(μ-oxo)diiron(IV) with two bridging formates, two terminal formates, and two imidazole ligands, also favors hydrogen-atom abstraction as the pathway for methane activation.[177] Attempts to find a transition state corresponding to another mechanism failed. By using a similar model for $MMOH_Q$, evidence was again presented for hydrogen-atom abstraction by a diiron(IV) species.[176] The resulting methyl radical interacts weakly with the iron atoms, which could explain the apparent short lifetime of radical intermediates calculated from radical-clock and chiral-ethane studies. It should be noted that, in the latter model, methane approaches the diiron core from a position that is not accessible in the protein active site.

A two-step concerted mechanism was proposed on the basis of a simple model for $MMOH_Q$ that is coordinatively unsaturated, a bis(μ-oxo)diiron(IV) core supported by a bridging formate with a hydroxide ligand on one iron and two hydroxides on the other iron atom.[179, 181, 211, 212] This diiron complex first forms a complex with methane, which is followed by hydrogen-atom abstraction via a four-center transition state to give an intermediate with a bridging hydroxide and an iron-bound methyl group. The methyl group then migrates to form a C–O bond with the bridging hydroxide and afford a methanol complex.

Most recently, DFT calculations were performed with the intention of trying to understand the mechanisms of both dioxygen and methane activation in sMMO.[182–184] By using a much larger model of the active site than previous studies, structures were predicted for the $MMOH_{peroxo}$, $MMOH_Q$, and putative $MMOH_{superoxo}$ intermediates (see Section 3). The model of $MMOH_Q$ used in this study has a bis(μ-oxo)diiron(IV) core, but it differs from other models in that the water molecule bound to Fe1 is not displaced by Glu243 (see Figure 13). The site distal to the two histidine ligands, which faces the hydrophobic substrate binding site, was the only position that was acceptable for methane approach to the diiron center. The only energetically reasonable reaction pathway for methane was a straight-on approach to the bridging oxygen atom (Figure 16). The calculated activation energy for this reaction is 13.2 kcal mol^{-1}, which is in reasonable agreement with the 9–12 kcal mol^{-1} obtained experimentally.[50, 147, 157, 209] In this transition state, the hydrogen atom facing the bridging oxide is partially bound to both oxygen and carbon (Figure 16). Interestingly, two different reaction pathways were identified that emerge from this starting point.

One pathway involves methyl radical recoil and formation of the O–H bond yielding a (μ-hydroxo)diiron center (①, Figure 16). In order for the methyl radical to rebound, the OH group must rotate and make a 93° angle with the C–O bond axis, a process calculated to take 5–10 ps. This time is sufficient for an ethyl radical in solution to racemize completely, but DFT calculations indicate that a steric clash between the CH_2 fragment and the newly formed O–H bond in the active site can significantly retard rotation around the C–C bond.[213]

A second, nonsynchronous concerted pathway was also identified that affords methanol from the transition state with a negligible energy barrier (②, Figure 16). In this mechanism, the O–H bond first shortens to 0.97 Å without breaking the partial bond to the methane carbon atom. Next the hydrogen atom rotates to make a 80–90° angle with the C–O axis while the carbon rotates in the opposite direction towards the oxygen atom. This entire process has a reaction barrier of only 1 kcal mol^{-1}.

The presence of two reaction channels with comparable activation energies can explain the partial retention of configuration observed with chiral ethane.[213] Products derived from the radical rebound channel undergo partial racemization, while those deriving from the concerted channel retain their configuration. The partitioning between these two reaction channels quantitatively accounts for the chiral ethane results and should be substrate dependent. Larger radical-clock substrates will favor the concerted mechanism because they have more difficulty reversing their trajectory to form a separate radical once the transition state is reached. A second study using a smaller set of 40 atoms also suggested the presence of two different pathways after initial hydrogen-atom abstraction, depending on the substrate.[184] Methylcyclopropane and ethane were computed to be immediately ionized after hydrogen atom abstraction to form a carbocation. The activation energy for final recombination of this carbocation to form a hydroxylated product is small. The reaction may even be described as nonsynchronous concerted. How important the radical recoil/rebound pathway is for methane remains to be established, but the finding that methyl radicals can be detected by using spin traps suggests that at least some methane oxidation may occur by this pathway.

Comparing the different calculational studies reveals that the predicted mechanism of methane activation is strongly dependent on the model selected for $MMOH_Q$ and the number of atoms used to describe it. Critical in the evaluation of these models is how well they relate to experimental results. In addition to reproducing the crystal structures for $MMOH_{ox}$ and $MMOH_{red}$, the largest DFT model does well in predicting reasonable values for the activation energy and in providing a rationale for seemingly contradictory results with mechanistic probe substrates.

Not only may substrates react with $MMOH_Q$ in different ways, but it is also possible that different substrates react with different oxygen intermediates, or that a single substrate reacts with different oxygen intermediates by different mechanisms. A linear relationship between the decay rate of $MMOH_{peroxo}$ and propene concentration has been observed for *M. capsulatus* (Bath), indicating that propene reacts directly with $MMOH_{peroxo}$.[147] No evidence for reaction of $MMOH_{peroxo}$ with propene was found in a study using the *M. trichosporium* OB3b enzyme, but the propene concentration used in this study may have been too low to observe its effect on the $MMOH_{peroxo}$ decay rate.[157] Additional support for propene oxidation by $MMOH_{peroxo}$ comes from the finding

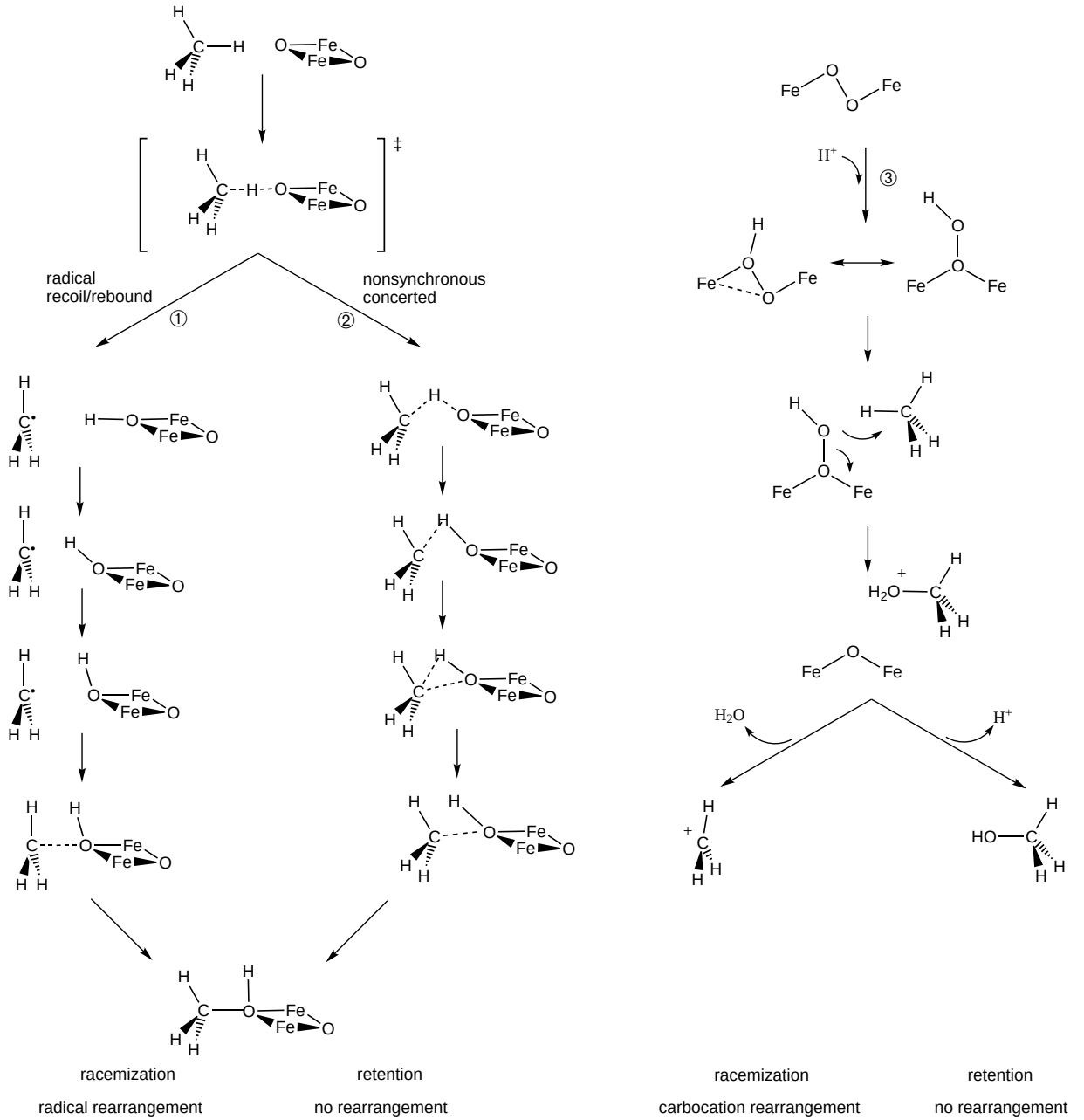

Figure 16. Model for the hydroxylation mechanism of MMO. The recoil/rebound and (nonsynchronous) concerted mechanisms (① and ②, respectively) are those suggested by recent DFT calculations.[183, 213] In addition, a mechanism for the involvement of $MMOH_{peroxo}$ in epoxidation and hydroxylation is suggested (③) based on related cytochrome P450 chemistry. The outcome of experiments with mechanistic probe substrates as predicted for each pathway is also depicted (First row: expected stereochemistry; second row: mechanistic probes).

that epoxidation of propene remains tightly coupled to NADH consumption, even at high MMOR:MMOH ratios, whereas uncoupling is observed with methane at MMOR:MMOH > 0.2.[27] Uncoupling probably occurs when MMOR provides additional electrons to either $MMOH_Q$ or $MMOH_{peroxo}$ to form H_2O and $MMOH_{ox}$. Propene reacts with $MMOH_{peroxo}$ and can thus compete with the oxidase reaction, whereas methane, which reacts only with $MMOH_Q$,[147] cannot.

Recent studies on cytochrome P450 have also provided evidence for the presence of more than one active oxygen intermediate.[214–218] Epoxidation of cyclohexene and 2-butene is enhanced at the expense of hydroxylation in site-directed mutants in which the proton transfer pathway responsible for the formation of the high-valent Fe^{IV}=O species is disrupted. The ferric hydroperoxide intermediate, which is still formed in these mutants, can epoxidize alkenes but is less active in hydroxylation reactions, which proceed primarily via the high-valent intermediate. It has been argued that the ferric hydroperoxide inserts OH^+ into substrates.[217, 219] Insertion of OH^+ into a C–H bond results in formation of a C–OH_2^+ unit, which can deprotonate to form an alcohol product or solvolyze to yield the carbocation product that has been detected with various substrate probes. Consistent with this

hypothesis is the finding that P450 mutants defective in forming compound I yield more carbocation-derived rearrangement products. Therefore, one explanation for the carbocation-derived products sometimes observed for MMO is that they react with a protonated peroxide intermediate prior to the formation of $MMOH_Q$ (③, Figure 16).[50, 145, 147]

5. Regulation of Catalysis by Component Interactions

The three protein components that comprise the soluble methane monooxygenase system orchestrate a series of electron-transfer and oxygen-activation reactions that result in the efficient and sustainable conversion of methane and dioxygen into methanol and water. The dynamic interactions between MMOH, MMOB, and MMOR are complex, and a detailed understanding of them is still incomplete. In this section we examine the various roles of component interactions in MMO catalysis and discuss what is known about the spatial and temporal relationships between the individual components.

An early and important illustration of the complexity of component interactions was the finding that steady-state hydroxylation rates increase with increasing MMOB concentration to a maximum at MMOB:MMOH = 2:1, but decrease at higher MMOB:MMOH ratios.[27, 44, 50] Recently several aspects of component interactions for the *M. capsulatus* (Bath) enzyme were investigated by using a combination of steady-state kinetic, calorimetric, and spectroscopic methods.[27] MMOR catalyzes the reduction of O_2 by NADH to H_2O_2 at relatively low rates in the absence of other MMO components. Addition of either MMOH, or MMOH and MMOB, increases the rate of oxidase activity but abolishes H_2O_2 formation, and O_2 is probably reduced completely to water. In the presence of methane, NADH oxidation and O_2 consumption are completely coupled to substrate hydroxylation at MMOR:MMOH < 0.2, whereas higher MMOR concentrations result in leakage of reducing equivalents in the form of oxidase activity. The steady-state hydroxylase and oxidase activities at various MMOB:MMOH and MMOR:MMOH ratios are best described by a model in which MMOB and MMOR bind noncompetitively at distinct sites on MMOH, both with a 2:1 stoichiometry.[27] This model yields K_d values for MMOB and MMOR binding in the 0.1 – 1 μM range, in good agreement with K_d values obtained by isothermal titration calorimetry. Kinetic information on MMOB and MMOR binding to MMOH has been obtained by stopped-flow fluorescence spectroscopy. Binding of MMOB and MMOR occurs in two steps, a rapid preequilibrium followed by a much slower isomerization equilibrium. Dissociation rate constants for the preequilibria of MMOH with MMOR (60 s^{-1} at 45 °C) and MMOB (26 s^{-1} at 45 °C) are significantly faster than the steady-state turnover rate for MMO.

Several important differences with regard to component interactions seem to exist between the enzymes from *M. capsulatus* (Bath) and *M. trichosporium* OB3b. Fluorescence titration studies on the enzyme from *M. trichosporium* OB3b showed the formation of a tight MMOB – MMOR complex ($K_d = 0.4$ μM),[44] whereas neither fluorescence spectroscopy nor isothermal titration calorimetry showed any evidence for complex formation between MMOB and MMOR for *M. capsulatus* (Bath).[27] Steady-state kinetic data for the *M. trichosporium* OB3b enzyme were interpreted by using a model in which MMOB and MMOR compete for binding sites on MMOH at high MMOB:MMOH ratios,[44] but a noncompetitive model was favored for *M. capsulatus* (Bath).[27] It is important to remember that *M. trichosporium* OB3b and *M. capsulatus* (Bath), although both methanotrophs, belong to evolutionarily distinct classes of bacteria. Differences between the two sMMO systems may be most prominent in component interactions.

MMOB and MMOR not only affect the rate and efficiency of catalysis by MMOH, but they also determine the regioselectivity of hydroxylation reactions.[46, 50] A study on the *M. trichosporium* OB3b enzyme found distinct product distributions for the oxygenation of isopentane by three different systems capable of oxygenation: I: MMOH, MMOR, NADH, and O_2; II: MMOH and H_2O_2; III: $MMOH_{red}$ and O_2 (single turnover).[46] Addition of as little as 0.1 mol equiv of MMOB changed the product distributions of systems I and III to one common outcome. Maximal rates for systems I and III were reached only at 1.5 – 2.0 MMOB per MMOH, however. In contrast, the hydrogen peroxide catalyzed system II was fully inhibited by MMOB at a 1:1 MMOB:MMOH ratio. Similar results have been reported for the hydrogen peroxide sustained hydroxylation by MMOH from *M. capsulatus* (Bath).[220]

There are several examples of the effect of component interactions on specific catalytic steps. MMOB enhances electron transfer rates between MMOR and MMOH.[27] As mentioned before, MMOB affects the kinetics of the dioxygen-activation reaction in such a way that several intermediates can be observed in its presence, whereas none are seen for the reaction of $MMOH_{red}$ alone with O_2. Reaction of $MMOH_{red}$ with O_2 is 1000-fold faster in the presence of MMOB.[49] The effect of different MMOB:MMOH ratios on the kinetics of $MMOH_Q$ formation and decay were interpreted to indicate that the presence of MMOB increases the formation rates of both $MMOH_{peroxo}$ and $MMOH_Q$, while decay of $MMOH_Q$ is relatively unaffected.[49] Various kinetic steps are also influenced by mutation of several amino acids in MMOB. Substitution of the conserved His 33 by alanine decreases the formation rate of $MMOH_{peroxo}$ by more than 50-fold. The quadruple mutant (N107G/S109A/S110A/T111A) has no effect on the formation rates for $MMOH_{peroxo}$ and $MMOH_Q$, but instead leads to a threefold increase in $MMOH_Q$ decay in the presence of larger substrates such as furan.[221] Studies on the enzyme from *M. trichosporium* OB3b also indicated that the presence of either 1.0 or 0.1 equivalents of MMOR decreases the O_2-induced decay rate of $MMOH_{red}$ in the MMOH:MMOB complex from 22 to 1.2 s^{-1}.[120] The rate of $MMOH_Q$ formation increases in the presence of 0.1 mole equivalents of MMOR, however, which means that, even in the presence of small quantities of reductase, formation of $MMOH_{peroxo}$ is no longer observed.[120]

The profound effects of MMOB and MMOR observed in both single-turnover reactions and in steady-state catalysis imply that component interactions affect the diiron active site. Both components affect the redox potentials $E_1^{o'}$ and $E_2^{o'}$ of MMOH.[2, 45, 48, 96, 120, 222] Binding of MMOB decreases the potential for both equilibria equally and substantially, which means that MMOB binds more tightly to $MMOH_{ox}$ than to $MMOH_{red}$. Binding of both MMOB and MMOR increases both potentials sharply in such a way that two-electron transfer becomes favored (*M. capsulatus* (Bath): $E_2^{o'} > E_1^{o'} \approx 100$ mV; *M. trichosporium* OB3b: $E_1^{o'} = 76$ mV $E_2^{o'} = 125$ mV, all potentials are relative to the normal hydrogen electrode).

Spectroscopic evidence for structural changes in the diiron site has been obtained only for MMOB binding. MMOR binding does not affect the spectroscopic properties of the diiron site. MMOB binding has only a subtle effect on EXAFS spectra.[93] MCD studies on $MMOH_{red}$ showed that MMOB disturbs the coordination geometry of one iron, probably that corresponding to Fe2 in the crystal structure of MMOH (see Section 2).[108–110] Binding of MMOB has been detected by EPR spectroscopy for all three oxidation states of MMOH.[44, 46, 98, 100] Titration of MMOB to $MMOH_{mv}$ showed full conversion into the spectrum of the MMOH:MMOB complex after addition of 1.7 MMOB per MMOH, which indicates a 1:2 binding stoichiometry. Surprisingly, only 0.6 mol equivalents of MMOB are needed to reach the same point for $MMOH_{red}$,[46] providing yet another example of a component effect that is maximal at substoichiometric ratios. Other illustrations of the same phenomenon include the effect of MMOB on substrate hydroxylation regioselectivity and the effects of MMOR on both the MMOH redox potential and the rate of $MMOH_{red}$ oxidation by O_2.[46, 120] All of these effects are indicative of hysteresis, which could occur when binding and dissociation of, for example, MMOR to $MMOH_{red}$ are faster than relaxation within MMOH from a complexed structure to its free conformational state. Therefore, a single molecule of MMOB or MMOR can service several molecules of MMOH. The 1:1:0.1 molar ratio of MMOH:MMOB:MMOR found in methanotrophic bacteria indicates that such hysteresis may be functionally important in vivo as well.[24, 51]

A detailed structural picture of the component complexes is currently unavailable, because no X-ray structure has yet been obtained. Chemical cross-linking experiments revealed that MMOB and MMOR bind to the α and β subunits of MMOH, respectively.[44] Small angle X-ray scattering experiments have been performed on *M. capsulatus* (Bath) sMMO to address whether or not significant conformational changes occur upon MMOB or MMOR binding to MMOH.[223] A major distortion of the MMOH structure was observed only when a 1:10:10 stoichiometry of MMOH:MMOB:MMOR was employed, ratios that are physiologically and functionally unreasonable. Addition of MMOB or MMOR, alone in a 1:2 ratio or together in a 1:2:2 stoichiometry, did not lead to structural distortions large enough to be detected by this technique. The model for the MMOH – MMOB complex that was discussed in Section 2.2 on the basis of NMR experiments is consistent with the X-ray scattering experiments, because binding of MMOB in the canyon region of MMOH is not expected to distort the overall ellipsoid form of MMOH. X-ray structure determinations of component complexes will be necessary to reveal the structural basis for component effects, however.

6. Summary and Outlook

A wide variety of methodologies derived from the disciplines of microbiology, enzymology, structural biology, and inorganic, physical, organic, and quantum chemistry have contributed to our current understanding of catalysis by the soluble methane monooxygenase system. High-resolution structures are available for two of the three protein components, MMOH and MMOB. Structural information about the diiron center in a variety of redox and complex states has provided important insights into the geometric flexibility that allows it to accommodate readily oxidation states ranging from $Fe^{II}Fe^{II}$ to $Fe^{IV}Fe^{IV}$. A unique feature of sMMO is that several intermediates in the dioxygen activation reaction build up sequentially before they decay, even in the absence of substrate, which has enabled a still incomplete molecular movie of dioxygen activation to be compiled. DFT calculations have begun to contribute new suggestions for the structures of oxygen intermediates and to provide insights into the reactions of these intermediates with substrates.

Although the basic sequence of events in dioxygen activation and substrate hydroxylation is now known, especially with regard to the role of the diiron center, other aspects of catalysis are less clear. One of these is the role of protein residues in formation of oxygen intermediates, electron and proton transfer, and substrate binding/access to the diiron active site. A high-yield recombinant expression system for MMOH would help to answer these questions by the application of site-directed mutagenesis. The recent finding that a fourth protein component (OrfY) exists in *M. capsulatus* (Bath) cells and interacts with MMOH raises the important question of its function in vivo.

Component interactions tightly control various reactions in the sMMO system. High-resolution structural information on MMOR and component complexes is required, however, to understand how component interactions regulate catalysis. For example, what structural changes in the vicinity of the $MMOH_{red}$ active site make it much more reactive toward dioxygen, and how does binding of MMOB at the surface of MMOH lead to those structural changes? More sophisticated programs and faster computers will allow the application of DFT and quantum mechanical molecular dynamics calculations using larger active site models and probing different aspects of MMO catalysis. More detailed structural information on $MMOH_{peroxo}$, $MMOH_Q$, and perhaps still undiscovered intermediates is crucial for providing well-defined starting structures for these calculations, however. An ultimate test for our understanding of MMO catalysis would be the successful design of a synthetic MMO model that catalyzes the hydroxylation of methane with an efficiency and specificity similar to that of the native enzyme.

This work was supported by a grant from the National Institute of General Medical Sciences. M.M. is a Human

Frontier of Science Program postdoctoral fellow. D.A.K. is supported by a National Institutes of Health Biotechnology Training Grant. J.L.B. is a Howard Hughes Medical Institute predoctoral fellow, and J.M. is a Feodor-Lynen postdoctoral fellow.

7. Appendix: Abbreviations

CD:	circular dichroism
CT1:	charge-transfer complex 1
CT2:	charge-transfer complex 2
DFT:	density functional theory
DMSO:	dimethyl sulfoxide
$E^{\circ\prime}$:	formal redox potential at pH 7.0
ENDOR:	electron-nuclear double resonance
EPR:	electron paramagnetic resonance
ESEEM:	electron-spin echo envelope modulation
EXAFS:	extended X-ray absorption fine structure
FAD:	flavin adenine dinucleotide
Fd:	ferredoxin
FMN:	flavin mononucleotide
FNR:	Fd – $NADP^+$ oxidoreductase
KIE:	kinetic isotope effect
MC1:	Michaelis complex 1
MCD:	magnetic circular dichroism
MMO:	methane monooxygenase
MMOB:	regulatory protein of sMMO
MMOH:	hydroxylase protein of sMMO
$MMOH_{DMSO}$:	complex of MMOH with DMSO
$MMOH_{mv}$:	MMOH in the mixed-valent $Fe^{III}Fe^{II}$ oxidation state
$MMOH_{ox}$:	MMOH in the $Fe^{III}Fe^{III}$ oxidation state
$MMOH_{peroxo}$:	peroxo intermediate in dioxygen activation, also named H_{peroxo} or compound P
$MMOH_Q$:	high-valent intermediate in dioxygen activation, also named compound Q
$MMOH_{Q_x}$:	one-electron reduced, $Fe^{III}Fe^{IV}$ form of $MMOH_Q$, formed by radiolytic reduction at 77 K
$MMOH_{red}$:	MMOH in the $Fe^{II}Fe^{II}$ oxidation state
$MMOH_{superoxo}$:	superoxo intermediate in dioxygen activation
MMOR:	reductase protein of sMMO
NAD^+:	nicotinamide adenine dinucleotide, oxidized form
NADH:	nicotinamide adenine dinucleotide, reduced form
$NADP^+$:	nicotinamide adenine dinucleotide phosphate, oxidized form
P2:	regulatory protein in phenol hydroxylase from *Pseudomonas* sp. CF600
PDR:	phthalate dioxygenase reductase
pMMO:	particulate methane monooxygenase
RFQ:	rapid freeze – quench
sMMO:	soluble methane monooxygenase
SQ:	semiquinone

Received: January 10, 2001
Revised: May 3, 2001 [A 442]

[1] A. L. Feig, S. J. Lippard, *Chem. Rev.* **1994**, *94*, 759 – 805.
[2] K. E. Liu, S. J. Lippard, *Adv. Inorg. Chem.* **1995**, *42*, 263 – 289.
[3] B. J. Wallar, J. D. Lipscomb, *Chem. Rev.* **1996**, *96*, 2625 – 2657.
[4] A. M. Valentine, S. J. Lippard, *J. Chem. Soc. Dalton Trans.* **1997**, 3925 – 3931.
[5] R. J. Deeth, H. Dalton, *J. Biol. Inorg. Chem.* **1998**, *3*, 302 – 306.
[6] L. Westerheide, M. Pascaly, B. Krebs, *Curr. Opin. Chem. Biol.* **2000**, *4*, 235 – 241.
[7] R. S. Hanson, T. E. Hanson, *Microbiol. Rev.* **1996**, *60*, 439 – 471.
[8] C. Anthony, *The Biochemistry of Methylotrophs*, Academic Press, London, **1982**.
[9] I. J. Higgins, D. J. Best, R. C. Hammond, *Nature* **1980**, *286*, 561 – 564.
[10] J. C. Murrell, *Biodegradation* **1994**, *5*, 145 – 159.
[11] J. C. Murrell, B. Gilbert, I. R. McDonald, *Arch. Microbiol.* **2000**, *173*, 325 – 332.
[12] H.-H. T. Nguyen, M. Zhu, S. J. Elliot, K. H. Nakagawa, B. Hedman, A. M. Costello, T. L. Peeples, B. Wilkinson, H. Morimoto, P. G. Williams, H. G. Floss, M. E. Lidstrom, K. O. Hodgson, S. I. Chan in *Microbial Growth on C_1 Compounds* (Eds.: M. E. Lidstrom, F. R. Tabita), Kluwer Academic, Dordrecht, **1996**, pp. 150 – 158.
[13] H.-H. T. Nguyen, K. H. Nakagawa, B. Hedman, S. J. Elliott, M. E. Lidstrom, K. O. Hodgson, S. I. Chan, *J. Am. Chem. Soc.* **1996**, *118*, 12766 – 12776.
[14] H.-H. T. Nguyen, S. J. Eliott, J. H.-K. Yip, S. I. Chan, *J. Biol. Chem.* **1998**, *273*, 7957 – 7966.
[15] M. Takeguchi, K. Miyakawa, I. Okura, *J. Mol. Catal. A* **1998**, *132*, 145 – 153.
[16] J. A. Zahn, A. A. DiSpirito, *J. Bacteriol.* **1996**, *178*, 1018 – 1029.
[17] J. Colby, D. I. Stirling, H. Dalton, *Biochem. J.* **1977**, *165*, 395 – 402.
[18] H. Dalton, *Adv. Appl. Microbiol.* **1980**, *26*, 71 – 87.
[19] J. Green, H. Dalton, *J. Biol. Chem.* **1989**, *264*, 17698 – 17703.
[20] B. G. Fox, J. G. Borneman, L. P. Wackett, J. D. Lipscomb, *Biochemistry* **1990**, *29*, 6419 – 6427.
[21] M. J. Rataj, J. E. Kauth, M. I. Donnelly, *J. Biol. Chem.* **1991**, *266*, 18684 – 18690.
[22] K. K. Andersson, W. A. Froland, S.-K. Lee, J. D. Lipscomb, *New J. Chem.* **1991**, *15*, 411 – 415.
[23] J. R. Bragg, R. C. Prince, E. J. Harner, R. M. Atlas, *Nature* **1994**, *368*, 413 – 418.
[24] B. G. Fox, W. A. Froland, J. E. Dege, J. D. Lipscomb, *J. Biol. Chem.* **1989**, *264*, 10023 – 10033.
[25] J. Colby, H. Dalton, *Biochem. J.* **1978**, *171*, 461 – 468.
[26] M. P. Woodland, H. Dalton, *J. Biol. Chem.* **1984**, *259*, 53 – 59.
[27] G. T. Gassner, S. J. Lippard, *Biochemistry* **1999**, *38*, 12768 – 12785.
[28] A. C. Rosenzweig, C. A. Frederick, S. J. Lippard, P. Nordlund, *Nature* **1993**, *366*, 537 – 543.
[29] A. C. Rosenzweig, P. Nordlund, P. M. Takahara, C. A. Frederick, S. J. Lippard, *Chem. Biol.* **1995**, *2*, 409 – 418.
[30] N. Elango, R. Radhakrishnan, W. A. Froland, B. J. Wallar, C. A. Earhart, J. D. Lipscomb, D. H. Ohlendorf, *Protein Sci.* **1997**, *6*, 556 – 568.
[31] S.-L. Chang, B. J. Wallar, J. D. Lipscomb, K. H. Mayo, *Biochemistry* **1999**, *38*, 5799 – 5812.
[32] K. J. Walters, G. T. Gassner, S. J. Lippard, G. Wagner, *Proc. Natl. Acad. Sci. USA* **1999**, *96*, 7877 – 7882.
[33] D. A. Whittington, S. J. Lippard, *J. Am. Chem. Soc.* **2001**, *123*, 827 – 838.
[34] P. R. Ortiz de Montellano in *Cytochrome P450: Structure, Mechanism, and Biochemistry* (Eds.: P. R. Ortiz de Montellano), Plenum, New York, **1995**, pp. 245 – 303.
[35] S. S. Stahl, S. J. Lippard in *Iron Metabolism: Inorganic Biochemistry and Regulatory Mechanims* (Eds.: G. C. Ferreira, J. J. G. Moura, R. Franco), Wiley-VCH, Weinheim, **1999**, pp. 303 – 321.
[36] J. B. Vincent, G. L. Olivier-Lilley, B. A. Averill, *Chem. Rev.* **1990**, *90*, 1447 – 1467.
[37] D. E. Edmondson, B. H. Huynh, *Inorg. Chim. Acta* **1996**, *252*, 399 – 404.
[38] D. M. Kurtz, Jr., *J. Biol. Inorg. Chem.* **1997**, *2*, 159 – 167.
[39] E. I. Solomon, T. C. Brunold, M. I. Davis, J. N. Kemsley, S.-K. Lee, N. Lehnert, F. Neese, A. J. Skulan, Y.-S. Yang, J. Zhou, *Chem. Rev.* **2000**, *100*, 235 – 349.

[40] J. Xiong, D. M. Kurtz, Jr., J. Ai, J. Sanders-Loehr, *Biochemistry* **2000**, *39*, 5117 – 5125.
[41] S. J. Lippard, J. M. Berg, Principles of Bioinorganic Chemistry, University Science Books, Mill Valley, CA, **1994**.
[42] J. Lund, M. P. Woodland, H. Dalton, *Eur. J. Biochem.* **1985**, *147*, 297 – 305.
[43] J. Lund, H. Dalton, *Eur. J. Biochem.* **1985**, *147*, 291 – 296.
[44] B. G. Fox, Y. Liu, J. E. Dege, J. D. Lipscomb, *J. Biol. Chem.* **1991**, *266*, 540 – 550.
[45] K. E. Liu, S. J. Lippard, *J. Biol. Chem.* **1991**, *266*, 12836 – 12839.
[46] W. A. Froland, K. K. Andersson, S.-K. Lee, Y. Liu, J. D. Lipscomb, *J. Biol. Chem.* **1992**, *267*, 17588 – 17597.
[47] B. G. Fox, M. P. Hendrich, K. K. Surerus, K. K. Andersson, W. A. Froland, J. D. Lipscomb, E. Münck, *J. Am. Chem. Soc.* **1993**, *115*, 3688 – 3701.
[48] K. E. Paulsen, Y. Liu, B. G. Fox, J. D. Lipscomb, E. Münck, M. T. Stankovich, *Biochemistry* **1994**, *33*, 713 – 722.
[49] Y. Liu, J. C. Nesheim, S.-K. Lee, J. D. Lipscomb, *J. Biol. Chem.* **1995**, *270*, 24662 – 24665.
[50] K. E. Liu, A. M. Valentine, D. Wang, B. H. Huynh, D. E. Edmondson, A. Salifoglou, S. J. Lippard, *J. Am. Chem. Soc.* **1995**, *117*, 10174 – 10185.
[51] S. Grosse, L. Laramee, K.-D. Wendlandt, I. R. McDonald, C. B. Miguez, H.-P. Kleber, *Appl. Environ. Microbiol.* **1999**, *65*, 3929 – 3935.
[52] A. C. Stainthorpe, J. C. Murrell, G. P. C. Salmond, H. Dalton, V. Lees, *Arch. Microbiol.* **1989**, *152*, 154 – 159.
[53] A. C. Stainthorpe, V. Lees, G. P. C. Salmond, H. Dalton, J. C. Murrell, *Gene* **1990**, *91*, 27 – 34.
[54] D. E. Coufal, J. L. Blazyk, D. A. Whittington, W. W. Wu, A. C. Rosenzweig, S. J. Lippard, *Eur. J. Biochem.* **2000**, *267*, 2174 – 2185.
[55] D. L. N. Cardy, V. Laidler, G. P. C. Salmond, J. C. Murrell, *Arch. Microbiol.* **1991**, *156*, 477 – 483.
[56] D. L. N. Cardy, V. Laidler, G. P. C. Salmond, J. C. Murrell, *Mol. Microbiol.* **1991**, *5*, 335 – 342.
[57] I. R. McDonald, H. Uchiyama, S. Kambe, O. Yagi, J. C. Murrell, *Appl. Environ. Microbiol.* **1997**, *63*, 1898 – 1904.
[58] T. Shigematsu, S. Hanada, M. Eguchi, Y. Kamagata, T. Kanagawa, R. Kurane, *Appl. Environ. Microbiol.* **1999**, *65*, 5198 – 5206.
[59] A. K. Nielsen, K. Gerdes, H. Degn, J. C. Murrell, *Microbiology* **1996**, *142*, 1289 – 1296.
[60] A. K. Nielsen, K. Gerdes, J. C. Murrell, *Mol. Microbiol.* **1997**, *25*, 399 – 409.
[61] C. A. West, G. P. C. Salmond, H. Dalton, J. C. Murrell, *J. Gen. Microbiol.* **1992**, *138*, 1301 – 1307.
[62] M. Merkx, S. J. Lippard, **2001**, unpublished results.
[63] J. Powlowski, J. Sealy, V. Shingler, E. Cadieux, *J. Biol. Chem.* **1997**, *272*, 945 – 951.
[64] G. R. Johnson, R. H. Olsen, *Appl. Environ. Microbiol.* **1995**, *61*, 3336 – 3346.
[65] R. H. Olsen, J. J. Kukor, B. Kaphammer, *J. Bacteriol.* **1994**, *176*, 3749 – 3756.
[66] A. M. Byrne, J. J. Kukor, R. H. Olsen, *Gene* **1995**, *154*, 65 – 70.
[67] G. M. Whited, D. T. Gibson, *J. Bacteriol.* **1991**, *173*, 3010 – 3016.
[68] K.-M. Yen, M. R. Karl, L. M. Blatt, M. J. Simon, R. B. Winter, P. R. Fausset, H. S. Lu, A. A. Harcourt, K. K. Chen, *J. Bacteriol.* **1991**, *173*, 5315 – 5327.
[69] K.-M. Yen, M. R. Karl, *J. Bacteriol.* **1992**, *174*, 7253 – 7261.
[70] J. D. Pikus, J. M. Studts, C. Achim, K. E. Kauffmann, E. Münck, R. J. Steffan, K. McClay, B. G. Fox, *Biochemistry* **1996**, *35*, 9106 – 9119.
[71] V. Shingler, F. C. H. Franklin, M. Tsuda, D. Holroyd, M. Bagdasarian, *J. Gen. Microbiol.* **1989**, *135*, 1083 – 1092.
[72] I. Nordlund, J. Powlowski, V. Shingler, *J. Bacteriol.* **1990**, *172*, 6826 – 6833.
[73] J. Powlowski, V. Shingler, *J. Bacteriol.* **1990**, *172*, 6834 – 6840.
[74] I. Nordlund, J. Powlowski, Å. Hagström, V. Shingler, *J. Gen. Microbiol.* **1993**, *139*, 2695 – 2703.
[75] H. Saeki, K. Furuhashi, *J. Ferment. Bioeng.* **1994**, *78*, 399 – 406.
[76] A. Miura, H. Dalton, *Biosci. Biotechnol. Biochem.* **1995**, *59*, 853 – 859.
[77] F. J. Small, S. A. Ensign, *J. Biol. Chem.* **1997**, *272*, 24913 – 24920.
[78] S. C. Gallagher, R. Cammack, H. Dalton, *Eur. J. Biochem.* **1997**, *247*, 635 – 641.
[79] N.-Y. Zhou, A. Jenkins, C. K. N. C. K. Chion, D. J. Leak, *FEBS Lett.* **1998**, *430*, 181 – 185.
[80] N.-Y. Zhou, A. Jenkins, C. K. N. C. K. Chion, D. J. Leak, *Appl. Environ. Microbiol.* **1999**, *65*, 1589 – 1595.
[81] B. G. Fox, J. Shanklin, J. Ai, T. M. Loehr, J. Sanders-Loehr, *Biochemistry* **1994**, *33*, 12776 – 12786.
[82] S. C. Gallagher, A. George, H. Dalton, *Eur. J. Biochem.* **1998**, *254*, 480 – 489.
[83] H. Brandstetter, D. A. Whittington, S. J. Lippard, C. A. Frederick, *Chem. Biol.* **1999**, *6*, 441 – 449.
[84] D. A. Kopp, G. T. Gassner, J. L. Blazyk, S. J. Lippard, **2001**, unpublished results.
[85] D. E. Coufal, J. L. Blazyk, M. Merkx, S. J. Lippard, **2001**, unpublished results.
[86] D. Jahng, T. K. Wood, *Appl. Environ. Microbiol.* **1994**, *60*, 2473 – 2482.
[87] D. Jahng, C. S. Kim, R. S. Hanson, T. K. Wood, *Biotechnol. Bioeng.* **1996**, *51*, 349 – 359.
[88] J. S. Lloyd, P. De Marco, H. Dalton, J. C. Murrell, *Arch. Microbiol.* **1999**, *171*, 364 – 370.
[89] J. S. Lloyd, R. Finch, H. Dalton, J. C. Murrell, *Microbiol.* **1999**, *145*, 461 – 470.
[90] A. Ericson, B. Hedman, K. O. Hodgson, J. Green, H. Dalton, J. G. Bentsen, R. H. Beer, S. J. Lippard, *J. Am. Chem. Soc.* **1988**, *110*, 2330 – 2332.
[91] J. DeWitt, B. Hedman, A. Ericson, K. O. Hodgson, J. Bentsen, R. Beer, S. J. Lippard, J. Green, H. Dalton, *Physica B* **1989**, *158*, 97 – 98.
[92] J. G. DeWitt, J. G. Bentsen, A. C. Rosenzweig, B. Hedman, J. Green, S. Pilkington, G. C. Papaefthymiou, H. Dalton, K. O. Hodgson, S. J. Lippard, *J. Am. Chem. Soc.* **1991**, *113*, 9219 – 9235.
[93] J. G. DeWitt, A. C. Rosenzweig, A. Salifoglou, B. Hedman, S. J. Lippard, K. O. Hodgson, *Inorg. Chem.* **1995**, *34*, 2505 – 2515.
[94] L. Shu, Y. Liu, J. D. Lipscomb, L. Que, Jr., *J. Biol. Inorg. Chem.* **1996**, *1*, 297 – 304.
[95] L. Shu, J. C. Nesheim, K. Kauffmann, E. Münck, J. D. Lipscomb, L. Que, Jr., *Science* **1997**, *275*, 515 – 518.
[96] M. P. Woodland, D. S. Patil, R. Cammack, H. Dalton, *Biochim. Biophys. Acta* **1986**, *873*, 237 – 242.
[97] M. P. Hendrich, E. Münck, B. G. Fox, J. D. Lipscomb, *J. Am. Chem. Soc.* **1990**, *112*, 5861 – 5865.
[98] A. Davydov, R. Davydov, A. Gräslund, J. D. Lipscomb, K. K. Andersson, *J. Biol. Chem.* **1997**, *272*, 7022 – 7026.
[99] J.-P. Willems, A. M. Valentine, R. Gurbiel, S. J. Lippard, B. M. Hoffman, *J. Am. Chem. Soc.* **1998**, *120*, 9410 – 9416.
[100] R. Davydov, A. M. Valentine, S. Komar-Panicucci, B. M. Hoffman, S. J. Lippard, *Biochemistry* **1999**, *38*, 4188 – 4197.
[101] M. P. Hendrich, B. G. Fox, K. K. Andersson, P. G. Debrunner, J. D. Lipscomb, *J. Biol. Chem.* **1992**, *267*, 261 – 269.
[102] V. J. DeRose, K. E. Liu, D. M. Kurtz, Jr., B. M. Hoffman, S. J. Lippard, *J. Am. Chem. Soc.* **1993**, *115*, 6440 – 6441.
[103] H. Thomann, M. Bernardo, J. M. McCormick, S. Pulver, K. K. Andersson, J. D. Lipscomb, E. I. Solomon, *J. Am. Chem. Soc.* **1993**, *115*, 8881 – 8882.
[104] C. J. Bender, A. C. Rosenzweig, S. J. Lippard, J. Peisach, *J. Biol. Chem.* **1994**, *269*, 15993 – 15998.
[105] B. M. Hoffman, B. E. Sturgeon, P. E. Doan, V. J. DeRose, K. E. Liu, S. J. Lippard, *J. Am. Chem. Soc.* **1994**, *116*, 6023 – 6024.
[106] V. J. DeRose, K. E. Liu, S. J. Lippard, B. M. Hoffman, *J. Am. Chem. Soc.* **1996**, *118*, 121 – 134.
[107] B. E. Sturgeon, P. E. Doan, K. E. Liu, D. Burdi, W. H. Tong, J. M. Nocek, N. Gupta, J. Stubbe, D. M. Kurtz, Jr., S. J. Lippard, B. M. Hoffman, *J. Am. Chem. Soc.* **1997**, *119*, 375 – 386.
[108] S. Pulver, W. A. Froland, B. G. Fox, J. D. Lipscomb, E. I. Solomon, *J. Am. Chem. Soc.* **1993**, *115*, 12409 – 12422.
[109] S. Pulver, W. A. Froland, B. G. Fox, J. D. Lipscomb, E. I. Solomon, *J. Am. Chem. Soc.* **1994**, *116*, 4529.
[110] S. C. Pulver, W. A. Froland, J. D. Lipscomb, E. I. Solomon, *J. Am. Chem. Soc.* **1997**, *119*, 387 – 395.
[111] B. G. Fox, K. K. Surerus, E. Münck, J. D. Lipscomb, *J. Biol. Chem.* **1988**, *263*, 10553 – 10556.

[112] B. G. Fox, J. D. Lipscomb, *Biochem. Biophys. Res. Commun.* **1988**, *154*, 165 – 170.
[113] P. Nordlund, B.-M. Sjöberg, H. Eklund, *Nature* **1990**, *345*, 593 – 598.
[114] M. A. Holmes, I. Le Trong, S. Turley, L. C. Sieker, R. E. Stenkamp, *J. Mol. Biol.* **1991**, *220*, 583 – 593.
[115] P. Nordlund, H. Eklund, *J. Mol. Biol.* **1993**, *232*, 123 – 164.
[116] R. E. Stenkamp, *Chem. Rev.* **1994**, *94*, 715 – 726.
[117] R. M. Davydov, S. Ménage, M. Fontecave, A. Gräslund, A. Ehrenberg, *J. Biol. Inorg. Chem.* **1997**, *2*, 242 – 255.
[118] R. M. Davydov, J. Smieja, S. A. Dikanov, Y. Zang, L. Que, Jr., M. K. Bowman, *J. Biol. Inorg. Chem.* **1999**, *4*, 292 – 301.
[119] K. K. Andersson, T. E. Elgren, L. Que, Jr., J. D. Lipscomb, *J. Am. Chem. Soc.* **1992**, *114*, 8711 – 8713.
[120] Y. Liu, J. C. Nesheim, K. E. Paulsen, M. T. Stankovich, J. D. Lipscomb, *Biochemistry* **1997**, *36*, 5223 – 5233.
[121] A. C. Rosenzweig, S. J. Lippard, *Acc. Chem. Res.* **1994**, *27*, 229 – 236.
[122] A. C. Rosenzweig, H. Brandstetter, D. A. Whittington, P. Nordlund, S. J. Lippard, C. A. Frederick, *Proteins* **1997**, *29*, 141 – 152.
[123] D. A. Whittington, M. H. Sazinsky, S. J. Lippard, *J. Am. Chem. Soc.* **2001**, *123*, 1794 – 1795.
[124] Y. Lindqvist, W. Huang, G. Schneider, J. Shanklin, *EMBO J.* **1996**, *15*, 4081 – 4092.
[125] A. Lombardi, C. M. Summa, S. Geremia, L. Randaccio, V. Pavone, W. F. DeGrado, *Proc. Natl. Acad. Sci. USA* **2000**, *97*, 6298 – 6305.
[126] M. E. Andersson, M. Högbom, A. Rinaldo-Matthis, K. K. Andersson, B.-M. Sjöberg, P. Nordlund, *J. Am. Chem. Soc.* **1999**, *121*, 2346 – 2352.
[127] W. C. Voegtli, N. Khidekel, J. Baldwin, B. A. Ley, J. M. Bollinger, Jr., A. C. Rosenzweig, *J. Am. Chem. Soc.* **2000**, *122*, 3255 – 3261.
[128] J. Stubbe, W. A. van der Donk, *Chem. Rev.* **1998**, *98*, 705 – 762.
[129] D. A. Whittington, A. C. Rosenzweig, C. A. Frederick, S. J. Lippard, *Biochemistry* **2001**, *40*, 3476 – 3482.
[130] G. M. Raner, L. J. Martins, W. R. Ellis, Jr., *Biochemistry* **1997**, *36*, 7037 – 7043.
[131] L. J. Martins, C. P. Hill, W. R. Ellis, Jr., *Biochemistry* **1997**, *36*, 7044 – 7048.
[132] J. Xiong, R. S. Phillips, D. M. Kurtz, Jr., S. Jin, J. Ai, J. Sanders-Loehr, *Biochemistry* **2000**, *39*, 8526 – 8536.
[133] C. S. Farmer, D. M. Kurtz, Jr., R. S. Phillips, J. Ai, J. Sanders-Loehr, *J. Biol. Chem.* **2000**, *275*, 17043 – 17050.
[134] Y. Shinohara, H. Uchiyama, O. Yagi, I. Kusakabe, *J. Ferment. Bioeng.* **1998**, *85*, 37 – 42.
[135] H. Hemmi, J. M. Studts, Y. K. Chae, J. Song, J. L. Markley, B. G. Fox, *Biochemistry* **2001**, *40*, 3512 – 3524.
[136] J. S. Lloyd, A. Bhambra, J. C. Murrell, H. Dalton, *Eur. J. Biochem.* **1997**, *248*, 72 – 79.
[137] H. Qian, U. Edlund, J. Powlowski, V. Shingler, I. Sethson, *Biochemistry* **1997**, *36*, 495 – 504.
[138] J. Colby, H. Dalton, *Biochem. J.* **1979**, *177*, 903 – 908.
[139] J. Green, H. Dalton, *Biochem. J.* **1989**, *259*, 167 – 172.
[140] R. C. Prince, R. N. Patel, *FEBS Lett.* **1986**, *203*, 127 – 130.
[141] C. C. Correll, C. J. Batie, D. P. Ballou, M. L. Ludwig, *Science* **1992**, *258*, 1604 – 1610.
[142] C. C. Correll, M. L. Ludwig, C. M. Bruns, P. A. Karplus, *Protein Sci.* **1993**, *2*, 2112 – 2133.
[143] G. Kurisu, M. Kusunoki, E. Katoh, T. Yamazaki, K. Teshima, Y. Onda, Y. Kimata-Ariga, T. Hase, *Nat. Struct. Biol.* **2001**, *8*, 117 – 121.
[144] K. Moffat, *Nat. Struct. Biol.* **1998**, *5*, 641 – 645.
[145] S.-K. Lee, J. C. Nesheim, J. D. Lipscomb, *J. Biol. Chem.* **1993**, *268*, 21569 – 21577.
[146] S.-K. Lee, B. G. Fox, W. A. Froland, J. D. Lipscomb, E. Münck, *J. Am. Chem. Soc.* **1993**, *115*, 6450 – 6451.
[147] A. M. Valentine, S. S. Stahl, S. J. Lippard, *J. Am. Chem. Soc.* **1999**, *121*, 3876 – 3887.
[148] J. D. Lipscomb, S.-K. Lee, J. C. Nesheim, Y. Jin, B. J. Wallar, X.-Y. Zhang in *Iron Metabolism: Inorganic Biochemistry and Regulatory Mechanisms* (Eds.: G. C. Ferreira, J. J. G. Moura, R. Franco), Wiley-VCH, Weinheim, **1999**, pp. 323 – 339.
[149] R. E. Blankenship, W. W. Parson, *Annu. Rev. Biochem.* **1978**, *47*, 635 – 653.
[150] J. E. Walker, *Q. Rev. Biophys.* **1992**, *25*, 253 – 324.
[151] G. T. Gassner, M. L. Ludwig, D. L. Gatti, C. C. Correll, D. P. Ballou, *FASEB J.* **1995**, *9*, 1411 – 1418.
[152] J. L. Blazyk, G. T. Gassner, S. J. Lippard, **2001**, unpublished results.
[153] S. S. Stahl, W. A. Francisco, M. Merkx, J. P. Klinman, S. J. Lippard, *J. Biol. Chem.* **2001**, *276*, 4549 – 4553.
[154] K. E. Liu, D. Wang, B. H. Huynh, D. E. Edmondson, A. Salifoglou, S. J. Lippard, *J. Am. Chem. Soc.* **1994**, *116*, 7465 – 7466.
[155] K. E. Liu, A. M. Valentine, D. Qiu, D. E. Edmondson, E. H. Appelman, T. G. Spiro, S. J. Lippard, *J. Am. Chem. Soc.* **1995**, *117*, 4997 – 4998.
[156] S.-K. Lee, J. D. Lipscomb, *Biochemistry* **1999**, *38*, 4423 – 4432.
[157] B. J. Brazeau, J. D. Lipscomb, *Biochemistry* **2000**, *39*, 13503 – 13515.
[158] K. E. Liu, A. M. Valentine, D. Qiu, D. E. Edmondson, E. H. Appelman, T. G. Spiro, S. J. Lippard, *J. Am. Chem. Soc.* **1997**, *119*, 11134.
[159] K. Kim, S. J. Lippard, *J. Am. Chem. Soc.* **1996**, *118*, 4914 – 4915.
[160] J. Hwang, C. Krebs, B. H. Huynh, D. E. Edmondson, E. C. Theil, J. E. Penner-Hahn, *Science* **2000**, *287*, 122 – 125.
[161] Q. Su, J. P. Klinman, *Biochemistry* **1998**, *37*, 12513 – 12525.
[162] W. A. Francisco, G. Tian, P. F. Fitzpatrick, J. P. Klinman, *J. Am. Chem. Soc.* **1998**, *120*, 4057 – 4062.
[163] A. L. Feig, A. Masschelein, A. Bakac, S. J. Lippard, *J. Am. Chem. Soc.* **1997**, *119*, 334 – 342.
[164] L. Que, Jr., *J. Chem. Soc. Dalton Trans.* **1997**, 3933 – 3940.
[165] J. Du Bois, T. J. Mizoguchi, S. J. Lippard, *Coord. Chem. Rev.* **2000**, *200*, 443 – 485.
[166] J. L. DuBois, M. J. Latimer, A. M. Valentine, S. S. Stahl, B. Hedman, S. J. Lippard, K. O. Hodgson, **2001**, unpublished results.
[167] E. I. Solomon, U. M. Sundaram, T. E. Machonkin, *Chem. Rev.* **1996**, *96*, 2563 – 2605.
[168] J. Cahoy, P. L. Holland, W. B. Tolman, *Inorg. Chem.* **1999**, *38*, 2161 – 2168.
[169] V. Mahadevan, R. J. M. Klein Gebbink, T. D. P. Stack, *Curr. Opin. Chem. Biol.* **2000**, *4*, 228 – 234.
[170] P. J. Riggs-Gelasco, L. Shu, S. Chen, D. Burdi, B. H. Huynh, L. Que, Jr., J. Stubbe, *J. Am. Chem. Soc.* **1998**, *120*, 849 – 860.
[171] B. E. Sturgeon, D. Burdi, S. Chen, B.-H. Huynh, D. E. Edmondson, J. Stubbe, B. M. Hoffman, *J. Am. Chem. Soc.* **1996**, *118*, 7551 – 7557.
[172] N. Ravi, J. M. Bollinger, Jr., B. H. Huynh, D. E. Edmondson, J. Stubbe, *J. Am. Chem. Soc.* **1994**, *116*, 8007 – 8014.
[173] D. Burdi, J.-P. Willems, P. Riggs-Gelasco, W. E. Antholine, J. Stubbe, B. M. Hoffman, *J. Am. Chem. Soc.* **1998**, *120*, 12910 – 12919.
[174] A. M. Valentine, P. Tavares, A. S. Pereira, R. Davydov, C. Krebs, B. M. Hoffman, D. E. Edmondson, B. H. Huynh, S. J. Lippard, *J. Am. Chem. Soc.* **1998**, *120*, 2190 – 2191.
[175] P. E. M. Siegbahn, M. R. A. Blomberg, *Annu. Rev. Phys. Chem.* **1999**, *50*, 221 – 249.
[176] H. Basch, K. Mogi, D. G. Musaev, K. Morokuma, *J. Am. Chem. Soc.* **1999**, *121*, 7249 – 7256.
[177] P. E. M. Siegbahn, *Inorg. Chem.* **1999**, *38*, 2880 – 2889.
[178] K. Yoshizawa, Y. Yokomichi, Y. Shiota, T. Ohta, T. Yamabe, *Chem. Lett.* **1997**, 587 – 588.
[179] K. Yoshizawa, T. Ohta, T. Yamabe, *Bull. Chem. Soc. Jpn.* **1998**, *71*, 1899 – 1909.
[180] K. Yoshizawa, T. Ohta, T. Yamabe, *Nippon Kagaku Kaishi* **1998**, 451 – 459.
[181] K. Yoshizawa, *J. Inorg. Biochem.* **2000**, *78*, 23 – 34.
[182] B. D. Dunietz, M. D. Beachy, Y. Cao, D. A. Whittington, S. J. Lippard, R. A. Friesner, *J. Am. Chem. Soc.* **2000**, *122*, 2828 – 2839.
[183] B. F. Gherman, B. D. Dunietz, D. A. Whittington, S. J. Lippard, R. A. Friesner, *J. Am. Chem. Soc.* **2001**, *123*, 3836 – 3837.
[184] P. E. M. Siegbahn, *J. Biol. Inorg. Chem.* **2001**, *6*, 27 – 45.
[185] B. F. Gherman, S. J. Lippard, R. A. Friesner, **2001**, unpublished results.
[186] N. D. Priestley, H. G. Floss, W. A. Froland, J. D. Lipscomb, P. G. Williams, H. Morimoto, *J. Am. Chem. Soc.* **1992**, *114*, 7561 – 7562.
[187] A. A. Shteinman, *J. Biol. Inorg. Chem.* **1998**, *3*, 325 – 330.
[188] E. Nordlander, K. K. Andersson, *J. Biol. Inorg. Chem.* **1998**, *3*, 300 – 301.
[189] P. E. M. Siegbahn, R. H. Crabtree, P. Nordlund, *J. Biol. Inorg. Chem.* **1998**, *3*, 314 – 317.
[190] D. A. Whittington, A. M. Valentine, S. J. Lippard, *J. Biol. Inorg. Chem.* **1998**, *3*, 307 – 313.

[191] K. Yoshizawa, *J. Biol. Inorg. Chem.* **1998**, *3*, 318 – 324.
[192] J. D. Lipscomb, L. Que, Jr., *J. Biol. Inorg. Chem.* **1998**, *3*, 331 – 336.
[193] A. M. Valentine, B. Wilkinson, K. E. Liu, S. Komar-Panicucci, N. D. Priestley, P. G. Williams, H. Morimoto, H. G. Floss, S. J. Lippard, *J. Am. Chem. Soc.* **1997**, *119*, 1818 – 1827.
[194] D. Griller, K. U. Ingold, *Acc. Chem. Res.* **1980**, *13*, 317 – 323.
[195] P. R. Ortiz de Montellano, R. A. Stearns, *J. Am. Chem. Soc.* **1987**, *109*, 3415 – 3420.
[196] M. Newcomb, *Tetrahedron* **1993**, *49*, 1151 – 1176.
[197] K. E. Liu, C. C. Johnson, M. Newcomb, S. J. Lippard, *J. Am. Chem. Soc.* **1993**, *115*, 939 – 947.
[198] A. M. Valentine, M.-H. Le Tadic-Biadatti, P. H. Toy, M. Newcomb, S. J. Lippard, *J. Biol. Chem.* **1999**, *274*, 10771 – 10776.
[199] Y. Jin, J. D. Lipscomb, *Biochim. Biophys. Acta* **2000**, *1543*, 47 – 59.
[200] F. Ruzicka, D.-S. Huang, M. I. Donnelly, P. A. Frey, *Biochemistry* **1990**, *29*, 1696 – 1700.
[201] S.-Y. Choi, P. E. Eaton, P. F. Hollenberg, K. E. Liu, S. J. Lippard, M. Newcomb, D. A. Putt, S. P. Upadhyaya, Y. Xiong, *J. Am. Chem. Soc.* **1996**, *118*, 6547 – 6555.
[202] S.-Y. Choi, P. E. Eaton, D. A. Kopp, S. J. Lippard, M. Newcomb, R. Shen, *J. Am. Chem. Soc.* **1999**, *121*, 12198 – 12199.
[203] Y. Jin, J. D. Lipscomb, *Biochemistry* **1999**, *38*, 6178 – 6186.
[204] N. Deighton, I. D. Podmore, M. C. R. Symons, P. C. Wilkins, H. Dalton, *J. Chem. Soc. Chem. Commun.* **1991**, 1086 – 1087.
[205] P. C. Wilkins, H. Dalton, I. D. Podmore, N. Deighton, M. C. R. Symons, *Eur. J. Biochem.* **1992**, *210*, 67 – 72.
[206] C. D. Ritchie, *Physical Organic Chemistry: The Fundamental Concepts*, Marcel Dekker, New York, **1990**, pp. 289 – 307.
[207] R. A. More O'Ferrall, *J. Chem. Soc. B* **1970**, 785 – 790.
[208] J. C. Nesheim, J. D. Lipscomb, *Biochemistry* **1996**, *35*, 10240 – 10247.
[209] E. A. Ambundo, S. J. Lippard, **2001**, unpublished results.
[210] P. E. M. Siegbahn, R. H. Crabtree, *J. Am. Chem. Soc.* **1997**, *119*, 3103 – 3113.
[211] K. Yoshizawa, T. Ohta, T. Yamabe, R. Hoffmann, *J. Am. Chem. Soc.* **1997**, *119*, 12311 – 12321.
[212] K. Yoshizawa, T. Ohta, Y. Shiota, T. Yamabe, *Chem. Lett.* **1997**, 1213 – 1214.
[213] V. Guallar, B. F. Gherman, S. J. Lippard, W. H. Miller, R. A. Friesner, **2001**, unpublished reults.
[214] A. D. N. Vaz, S. J. Pernecky, G. M. Raner, M. J. Coon, *Proc. Natl. Acad. Sci. USA* **1996**, *93*, 4644 – 4648.
[215] P. H. Toy, M. Newcomb, M. J. Coon, A. D. N. Vaz, *J. Am. Chem. Soc.* **1998**, *120*, 9718 – 9719.
[216] A. D. N. Vaz, D. F. McGinnity, M. J. Coon, *Proc. Natl. Acad. Sci. USA* **1998**, *95*, 3555 – 3560.
[217] M. Newcomb, P. H. Toy, *Acc. Chem. Res.* **2000**, *33*, 449 – 455.
[218] M. Newcomb, R. Shen, S.-Y. Choi, P. H. Toy, P. F. Hollenberg, A. D. N. Vaz, M. J. Coon, *J. Am. Chem. Soc.* **2000**, *122*, 2677 – 2686.
[219] M. Newcomb, M.-H. Le Tadic-Biadatti, D. L. Chestney, E. S. Roberts, P. F. Hollenberg, *J. Am. Chem. Soc.* **1995**, *117*, 12085 – 12091.
[220] Y. Jiang, P. C. Wilkins, H. Dalton, *Biochim. Biophys. Acta* **1993**, *1163*, 105 – 112.
[221] B. J. Wallar, J. D. Lipscomb, *Biochemistry* **2001**, *40*, 2220 – 2233.
[222] J. Kazlauskaite, H. A. O. Hill, P. C. Wilkins, H. Dalton, *Eur. J. Biochem.* **1996**, *241*, 552 – 556.
[223] S. C. Gallagher, A. J. Callaghan, J. Zhao, H. Dalton, J. Trewhella, *Biochemistry* **1999**, *38*, 6752 – 6760.
[224] A. C. Rosenzweig, C. A. Frederick, S. J. Lippard in *Microbial Growth on C_1 Compounds* (Eds.: M. E. Lidstrom, F. R. Tabita), Kluwer, Dordrecht, **1996**, pp. 141 – 149.
[225] J. M. Bollinger, Jr., C. Krebs, A. Vicol, S. Chen, B. A. Ley, D. E. Edmondson, B. H. Huynh, *J. Am. Chem. Soc.* **1998**, *120*, 1094 – 1095.
[226] P. Moënne-Loccoz, J. Baldwin, B. A. Ley, T. M. Loehr, J. M. Bollinger, Jr., *Biochemistry* **1998**, *37*, 14659 – 14663.
[227] J. A. Broadwater, J. Ai, T. M. Loehr, J. Sanders-Loehr, B. G. Fox, *Biochemistry* **1998**, *37*, 14664 – 14671.
[228] J. A. Broadwater, C. Achim, E. Münck, B. G. Fox, *Biochemistry* **1999**, *38*, 12197 – 12204.
[229] A. S. Pereira, W. Small, C. Krebs, P. Tavares, D. E. Edmondson, E. C. Theil, B. H. Huynh, *Biochemistry* **1998**, *37*, 9871 – 9876.
[230] P. Moënne-Loccoz, C. Krebs, K. Herlihy, D. E. Edmondson, E. C. Theil, B. H. Huynh, T. M. Loehr, *Biochemistry* **1999**, *38*, 5290 – 5295.
[231] R. Koradi, M. Billeter, K. Wüthrich, *J. Mol. Graphics* **1996**, *14*, 51 – 55.
[232] P. J. Kraulis, *J. Appl. Crystallogr.* **1991**, *24*, 946 – 950.
[233] E. A. Merritt, M. E. P. Murphy, *Acta Crystallogr. Sect. D* **1994**, *50*, 869 – 873.
[234] D. A. Whittington, S. J. Lippard in *Handbook of Metalloproteins* (Eds.: A. Messerschmidt, R. Huber, T. Poulos, K. Wieghardt), Wiley, Chichester, **2001**, pp. 712 – 724.
[235] T. A. Jones, J.-Y. Zou, S. W. Cowan, M. Kjeldgaard, *Acta Crystallogr. Sect. A* **1991**, *47*, 110 – 119.
[236] A. J. Nicholls, *GRASP Manual*, Columbia University, New York, **1993**.